Georgia Institute of Technology

AE 8900: Special Problems

Coulomb-Force Based Control Methods for an *n*-Spacecraft Reconfiguration Maneuver

Author: Jason C. Swenson

Advisor: Dr. Glenn Lightsey

April 20, 2018

Coulomb-Force Based Control Methods for an n-Spacecraft Reconfiguration Maneuver

Jason C. Swenson* and E. Glenn Lightsey†
Georgia Institute of Technology, Atlanta, GA, 30313

In an electrically-charged space plasma environment, spacecraft Coulomb forces are shown as a potential propellant-free alternative for an n-spacecraft formation reconfiguration maneuver with n_d deputy spacecraft. Two Coulomb force based methods (and one method without Coulomb forces) for reconfiguration maneuvers are developed, tested, and evaluated. Method 1a applies Direct Multiple Shooting in order to calculate the optimal thrust inputs of a minimum fuel trajectory. Method 1b uses the results from Method 1a to compare the optimal thrust input to the set of all possible resultant Coulomb force vectors at each point in time along a trajectory. Method 2, formulated from optimal control theory, solves directly for n_d spacecraft charge states at each point in time with Clohessy-Wiltshire relative dynamics and minimizes the final relative state vector error. The overall performance of Method 2 is shown to be superior than that of Method 1b in terms of both relative state vector error and total computational time. Furthermore, Method 2 shows performance comparable to the optimal minimum fuel trajectory calculated in Method 1a.

Abbreviations

BFGS	=	Broyden-Fletcher-Goldfarb-Shanno
BVP	=	Boundary Value Problem
CMP	=	Constrained Minimization Problem
CW	=	Clohessy-Wiltshire
DMS	=	Direct Multiple-Shooting
ECI	=	Earth-Centered Inertial
FONC	=	First-Order Necessary Conditions
ISS	=	International Space Station
LEO	=	Low-Earth Orbit
LVLH	=	Local-Vertical, Local-Horizontal
GEO	=	Geosynchronous Equatorial Orbit
KKT	=	Karush-Kuhn-Tucker
MOE	=	Mean Orbital Elements
NDS	=	Nonlinear Dynamical System
OCP	=	Optimal Control Problem
PMP	=	Pontryagin's Maximum Principle
RK	=	Runge-Kutta
SQP	=	Sequential Quadratic Programming

Nomenclature

a	=	semi-major axis
C_j	=	set of possible charge states for j^{th} deputy spacecraft
$c_j(t_i)$	=	charge state of j^{th} deputy spacecraft at time t_i
$\mathbf{d}$	=	disturbance vector

*Graduate Student, Guggenheim School of Aerospace Engineering, 270 Ferst Drive, Atlanta, GA 30313, USA
†Professor, Guggenheim School of Aerospace Engineering, 270 Ferst Drive, Atlanta, GA 30313, USA

e = eccentricity
$\mathbf{F}_{j,k}(t_i)$ = force vector of j^{th} deputy spacecraft on the k^{th} deputy spacecraft
$\mathbf{F}_{R,j}(t_i)$ = resultant Coulomb force vector of j^{th} deputy spacecraft at time t_i
$\mathbf{F}_R^*(t_i)$ = set of optimal resultant Coulomb forces for all deputy spacecraft at time t_i
f = true anomaly, function
g = inequality constraint
$\mathcal{H}$ = Hamiltonian
h = orbit altitude, equality constraint, step size
$\mathbf{h}$ = angular momentum vector
i = inclination
k_e = Coulomb's constant ($k_e = 8.99 \times 10^9 \frac{N \cdot m^2}{C^2}$)
$\mathcal{L}$ = Lagrangian
$\ell_j(t_i)$ = LVLH position vector of j^{th} deputy spacecraft at time t_i
$\dot{\ell}_j(t_i)$ = LVLH velocity vector of j^{th} deputy spacecraft at time t_i
$\boldsymbol{\lambda}_j(t_i)$ = co-state of j^{th} deputy spacecraft at time t_i
M = number of sub-nodes
N = number of nodes
n = mean motion, total number of spacecraft
n_d = number of deputy spacecraft
Ω = longitude of ascending node
ω = argument of periapsis
ω_A^B = angular velocity of frame B relative to frame A
$\mathfrak{oe}$ = set of orbital elements
Ψ = terminal cost
$q_j(t_i)$ = charge of j^{th} deputy spacecraft at time t_i
$\mathbf{R}$ = ECI position vector
$\dot{\mathbf{R}}$ = ECI velocity vector
R_{eq} = equatorial radius of the Earth
$\mathbf{r}_{j,k}(t_i)$ = position vector from j^{th} deputy spacecraft to k^{th} deputy spacecraft at time t_i
$\mathbf{t}$ = time vector
T = total time
t_0 = initial time
t_f = final time
θ_0 = angle formed by chief-centered frame and deputy-fixed frame
$\theta_j(t_i)$ = angle between optimal thrust input and resultant Coulomb force for j^{th} deputy spacecraft at time t_i
$\mathbf{u}$ = control input vector
$\mathbf{u}^*$ = optimal control thrust input vector
$\tilde{\mathbf{u}}^*$ = optimal Coulomb force control input vector
$\mathbf{x}_j(t_i)$ = LVLH vector of j^{th} deputy spacecraft at time t_i
$\mathbf{x}_{d,j}$ = desired state of j^{th} deputy spacecraft at time t_i
$\mathbf{x}_{0,j}$ = initial state of of j^{th} deputy spacecraft at time t_0
$\mathbf{x}_{f,j}$ = initial state of of j^{th} deputy spacecraft at time t_f

I. Introduction

NASA continues to identify precision formation flying as a "transformational" technology for future science missions to planets, asteroids, and other bodies within our Solar System [1]. With respect to precision formation flying, robust and autonomous relative state vector control for reconfiguration maneuvers is a problem that continues to be addressed in unique ways. [2–28] That is, how can each agent within a satellite formation be optimally controlled in order to achieve and maintain its final desired position and velocity state (relative to a chief or barycenter of the formation)?

While most formation flying scenarios rely heavily on micro-thrusters for precise relative position control, the use of resultant Coulomb forces produced between pairs of electrically-charged spacecraft may provide a propellant-free

alternative for controlling a close formation during a reconfiguration maneuver. Through the use of Coulomb forces within a formation, all spacecraft can save a significant amount of fuel.

The use of Coulomb forces is particularly well-suited for satellites in a formation on the order of meters apart. In a close formation, spacecraft relative positions are not heavily influenced by the effects of Earth oblation, short- and long-term secular orbit effects, and other perturbations.

The Coulomb force is found from Coulomb's Law. Coulomb's Law states that the force of two electrically-charged particles is proportional to Coulomb's constant. Coulomb's Law states that the product of both charges and inversely proportional to the square of the distance between the particles. Propulsive Coulomb forces arise from the interaction of two electrically-charged spacecraft with repelling (or attracting) electric fields. The spacecraft becomes electrically-charged as the influx of negatively-charged electrons exceeds the influx of positively-charged protons in a space plasma environment [29]. As King et. al. states, "The interaction arises from Coulomb forces between vehicles in a swarm of electrically charged spacecraft. Forces can be produced as a result of natural charging due to space plasma interaction. In the case of natural charging, the Coulomb forces represent perturbations on vehicles in the formation that onboard thrusters must counteract." [5]

A spacecraft's ability to effectively use Coulomb forces for relative position control is highly dependent upon the space plasma environment. The space plasma environment differs at Low Earth Orbit (LEO), Geostationary Orbit (GEO), and interplanetary space. In a GEO orbit, plasma exhibits lower densities and higher temperatures, yielding a large Debye length on the order of tens of meters. In a LEO orbit, the plasma exhibits higher densities and lower temperatures, yielding a Debye length on the order of meters. The allowable separation for the use of Coulomb forces for position control is approximately two effective Debye lengths or less. [24]

This paper investigates a proposed controller that uses Coulomb forces to control several satellites within a close formation with separation distances on the order of meters. Section II introduces useful theory for the problem and introduces dynamics for simulating the relative position between spacecraft. Section III details the methodology used for the problem, with particular attention paid to optimization and optimal control techniques. Section IV displays simulation results for a four-spacecraft formation and discusses the validity of the results. Section V finishes with concluding remarks and future work.

II. Theory

A. Relative Orbit Dynamics

In the chief-fixed Local-Vertical, Local-Horizontal (LVLH) reference frame, the nonlinear equations of relative motion [21] are used to analyze the relative motion of the spacecraft (e.g. a "deputy" spacecraft) relative to a primary, centralized spacecraft (e.g. a "chief" spacecraft). Let $\dot{\theta}_0$ be the rate of change of the angle formed by the chief-fixed LVLH frame and $\hat{I}$ component of the ECI frame, defined such that $\omega_0 = [0, 0, \dot{\theta}_0]$. The nonlinear equations of relative motion with disturbance vector, **d**, and control input vector, **u** are:

$$\ddot{x} = 2\dot{\theta}_0\dot{y} + \ddot{\theta}_0 y + \dot{\theta}_0{}^2 x - \frac{\mu(R_0 + x)}{((R_0 + x)^2 + y^2 + z^2)^{3/2}} + \frac{\mu}{R_0^2} + d_x + u_x \tag{1}$$

$$\ddot{y} = -2\dot{\theta}_0\dot{x} - \ddot{\theta}_0 x + \dot{\theta}_0{}^2 y - \frac{\mu y}{((R_0 + x)^2 + y^2 + z^2)^{3/2}} + d_y + u_y \tag{2}$$

$$\ddot{z} = -\ddot{\theta}_0 x + \dot{\theta}_0{}^2 y - \frac{\mu z}{((R_0 + x)^2 + y^2 + z^2)^{3/2}} + d_z + u_z \tag{3}$$

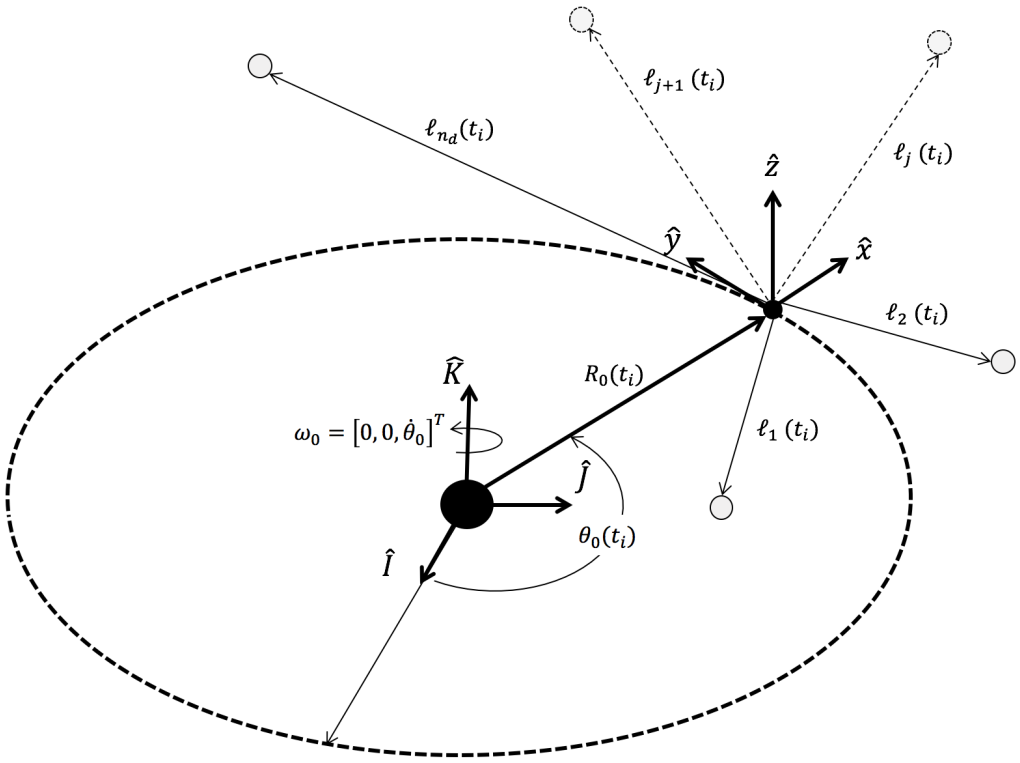

Fig. 1 Chief-fixed LVLH Frame. The LVLH frame is a rotating frame fixed at the chief. The relative positions (and velocities) of the n_d deputy spacecraft are resolved in the chief-fixed LVLH frame.

Figure 1 shows the chief-fixed LVLH frame. Note that $\ell_j(t_i) = [x_j, y_j, z_j]^T$. The set of nonlinear equations can be linearized into the linearized equations of relative motion. From the origin of the chief-fixed LVLH frame, the deputy spacecraft relative dynamics can be expressed as:

$$\ddot{x} = 2\dot{\theta}\dot{y} + (\dot{\theta}^2 + 2\frac{\mu}{R_0^3})x + \ddot{\theta}_0 y \tag{4}$$

$$\ddot{y} = -2\dot{\theta}\dot{x} + \ddot{\theta}_0 \dot{x} - (\dot{\theta}^2 - \frac{\mu}{R_0^3})y \tag{5}$$

$$\ddot{z} = -\frac{\mu}{R_0^3} z \tag{6}$$

For circular orbits, the linear equations of relative motion can be simplified further with the following assumptions: $\dot{\theta}_0 = n$ (where n is the mean motion) and $\ddot{\theta}_0 \approx 0$. The linearized equations are known collectively as the Clohessy-Wiltshire (CW) equations. Below are the CW equations for a circular orbit with disturbance vector, **d**, and control input vector, **u** incorporated:

$$\ddot{x} = 2n\dot{y} + 3n^2 x + d_x + u_x \tag{7}$$

$$\ddot{y} = -2n\dot{x} + d_y + u_y \tag{8}$$

$$\ddot{z} = -n^2 z + d_z + u_z \tag{9}$$

B. Optimization

1. Constrained Minimization Problem

The standard form of the constrained minimization problem (CMP) is formulated with an objective function $f(\mathbf{x}) : \mathbb{R}^n \to \mathbb{R}$, where $\mathbf{x} = \begin{bmatrix} x_1, & x_2, & \ldots, & x_n \end{bmatrix}^T \in \mathbb{R}^n$. In the CMP, there are j inequality constraints, m equality constraints and i side constraints. The CMP in standard form is represented as:

$$\begin{aligned} \min_{\mathbf{x}} \quad & \mathrm{f}(\mathbf{x}) \\ \text{subject to} \quad & g_j(\mathbf{x}) \leq 0, \text{ for } j = 1, \ldots, l, \\ & h_k(\mathbf{x}) = 0, \text{ for } k = 1, \ldots, m, \\ & \mathrm{lb}_i \leq x_i \leq \mathrm{ub}_i, \text{ for } i = 1, \ldots, n. \end{aligned} \tag{10}$$

where $g_j(\mathbf{x}) : \mathbb{R}^n \to \mathbb{R}$ are the j inequality constraints, $h_m(\mathbf{x}) : \mathbb{R}^n \to \mathbb{R}$ are the m equality constraints, and lb_i and ub_i represent the i lower and upper side constraints, respectively, on each design variable x_i.

2. Sequential Quadratic Programming

Sequential Quadratic Programming (SQP) is a method of finding the global minimum through successive quadratic approximations of the objective function. In an SQP problem, the constraints are linearized.

$$\begin{aligned} \min_{\mathbf{x}} \quad & \frac{1}{2}\mathbf{x}^T H \mathbf{x} + \mathbf{f}^T \mathbf{x} \\ \text{subject to} \quad & A(\mathbf{x}) = b \end{aligned} \tag{11}$$

In order to solve the SQP, the Lagrangian $\mathcal{L} = \left(\frac{1}{2}\mathbf{x}^T H \mathbf{x} + \mathbf{f}^T \mathbf{x}\right) + \boldsymbol{\lambda}^T (A\mathbf{x} - \mathbf{b})$ is formed. Note that $\mathbf{x}$ is an arbitrary vector in this case and may include both states and control inputs. The Karush-Kuhn-Tucker (KKT) conditions on $\mathcal{L}$ is: $\nabla_x \mathcal{L} = (G\mathbf{x}^* + \mathbf{c}) + \left(A^T \boldsymbol{\lambda}^*\right) = 0$. $A\mathbf{x}^* - \mathbf{b} = 0$ must also be satisfied. Then, the following linear system can be easily implemented and solved successively:

$$\begin{bmatrix} G & A^T \\ A & 0 \end{bmatrix} \begin{bmatrix} \mathbf{x}^* \\ \boldsymbol{\lambda}^* \end{bmatrix} = \begin{bmatrix} -\mathbf{c} \\ \mathbf{b} \end{bmatrix} \tag{12}$$

In this research, the MATLAB function **fmincon** is applied and is based on SQP.

C. Optimal Control

1. Optimal Control Problem

Given the nonlinear dynamical system (NDS) $\dot{\mathbf{x}} = f(\mathbf{x}, \mathbf{u})$, the Optimal Control Problem (OCP) aims to minimize the cost function, $J(\mathbf{x}(t), \mathbf{u}(t), t)$, based on the state, $\mathbf{x}(t)$ and/or control inputs, $\mathbf{u}(t)$ of the system.

The OCP with Lagrange multipliers [30]is described as:

$$\begin{aligned} \min_{\mathbf{u}} \quad & \int_{t_0}^{t_f} \left(\mathcal{L}(\mathbf{x}, \mathbf{u}, t) + \boldsymbol{\lambda}^T [\dot{\mathbf{x}} - f(\mathbf{x}, \mathbf{u}, t)]\right) \mathrm{dt} + \Psi(\mathbf{x}_f, t_f) \\ \text{subject to} \quad & \dot{\mathbf{x}} = f(\mathbf{x}, \mathbf{u}, t) \\ & \mathbf{x}(t_0) = \mathbf{x}_0 \end{aligned} \tag{13}$$

The Lagrangian is also known as the "running cost" function for the OCP and can include both states and control inputs. The First-Order Necessary Conditions (FONC) for optimality are described as:

$$\dot{\boldsymbol{\lambda}} = -\frac{\partial \mathcal{L}^T}{\partial \mathbf{x}} - \frac{\partial f^T}{\partial \mathbf{x}}\boldsymbol{\lambda} \tag{14}$$

$$\boldsymbol{\lambda}(t_f) = \left.\frac{\partial \Psi^T}{\partial \mathbf{x}}\right|_{\mathbf{x}_f, t_f} \tag{15}$$

$$0 = \frac{\partial \mathcal{L}}{\partial \mathbf{u}} + \boldsymbol{\lambda}^T \frac{\partial f}{\partial \mathbf{u}} \tag{16}$$

Equations 14-16 represented the co-state dynamics, co-state boundary condition, and optimal control policy, respectively. Let the Hamiltonian be $\mathcal{H} = \mathcal{L}(\mathbf{x}, \mathbf{u}, t) + \boldsymbol{\lambda}^T f(\mathbf{x}, \mathbf{u}, t)$. Then:

$$\dot{\boldsymbol{\lambda}} = -\frac{\partial \mathcal{H}^T}{\partial \mathbf{x}} \tag{17}$$

$$\boldsymbol{\lambda}(t_f) = \left.\frac{\partial \Psi^T}{\partial \mathbf{x}}\right|_{\mathbf{x}_f, t_f} \tag{18}$$

$$0 = \frac{\partial \mathcal{H}}{\partial \mathbf{u}} \tag{19}$$

The optimal control $\mathbf{u}^*$ is found by solving Equation 19. Denoting the Hamiltonian obtained from $\mathbf{u}^*$ as $\mathcal{H}^*$ yields:

$$\dot{\boldsymbol{\lambda}} = -\frac{\partial \mathcal{H}^{*\,T}}{\partial \mathbf{x}} \tag{20}$$

$$\boldsymbol{\lambda}(t_f) = \left.\frac{\partial \Psi^T}{\partial \mathbf{x}}\right|_{\mathbf{x}_f, t_f} \tag{21}$$

$$\dot{\mathbf{x}} = f(\mathbf{x}, \mathbf{u}^*, t) = \frac{\partial \mathcal{H}^*}{\partial \boldsymbol{\lambda}} \tag{22}$$

$$\mathbf{x}(t_0) = \mathbf{x_0} \tag{23}$$

Equations 20 - 23 show that the OCP can now be formulated and solved as a two-point boundary value problem (BVP) with a terminal cost function $\Psi(\mathbf{x}(t_f), t_f)$.

2. Direct Multiple-Shooting

The set of control inputs can be typically solved as a set of differential equations based on time t for simple dynamics. However, for complex, nonlinear dynamics, the Direct Multiple-Shooting (DMS) method can be applied to solve the OCP.

In DMS, the time interval $t \in [t_0, t_f]$ is first partitioned into N nodes ($N-1$ intervals). Then, the original BVP for $t_f = t_{N-1}$ becomes:

$$\begin{cases} \dot{\mathbf{x}}\left(t_0, t_1\right) & = f\left(\mathbf{x}\left(t_0, t_1\right),\ \mathbf{u}\left(t_0, t_1\right)\right),\ \mathbf{x}(t_0) = \mathbf{a_0},\ \mathbf{x}(t_1) = \mathbf{b_0} \\ \dot{\mathbf{x}}\left(t_1, t_2\right) & = f\left(\mathbf{x}\left(t_1, t_2\right),\ \mathbf{u}\left(t_1, t_2\right)\right),\ \mathbf{x}(t_1) = \mathbf{a_1},\ \mathbf{x}(t_2) = \mathbf{b_1} \\ & \vdots \\ \dot{\mathbf{x}}\left(t_{k-1}, t_k\right) & = f\left(\mathbf{x}\left(t_{k-1}, t_k\right),\ \mathbf{u}\left(t_{k-1}, t_k\right)\right),\ \mathbf{x}(t_{k-1}) = \mathbf{a_{k-1}},\ \mathbf{x}(t_k) = \mathbf{b_{k-1}} \\ & \vdots \\ \dot{\mathbf{x}}\left(t_{N-2}, t_{N-1}\right) & = f\left(\mathbf{x}\left(t_{N-2}, t_{N-1}\right),\ \mathbf{u}\left(t_{N-2}, t_{N-1}\right)\right),\ \mathbf{x}(t_{N-2}) = \mathbf{a_{N-2}},\ \mathbf{x}(t_{N-1}) = \mathbf{b_{N-2}} \end{cases} \tag{24}$$

For each time interval $t \in (t_k, t_{k+1})$, the successive solutions for both $x\left(t_k, t_{k+1}\right)$ and $u\left(t_k, t_{k+1}\right)$ can be pieced together to create a trajectory from t_0 to t_N for all $\mathbf{x}\left(t\right)$ and $\mathbf{u}\left(t\right)$. Equality constraints are also enforced between iterations in DMS with $a_k = b_{k-1}$.

3. Cost Functions

Minimum Fuel

With respect to fuel minimization, a common cost function to use is:

$$J(\mathbf{x}, \mathbf{u}) = \int_{t_0}^{t_f} \|\mathbf{u}(\mathbf{t})\|^2 \, \mathrm{dt} \tag{25}$$

Furthermore, for n spacecraft (operating in a continuous time domain), the cost function can be adapted as follows:

$$J(\mathbf{x}, \mathbf{u}) = \sum_{j=1}^{n} \int_{t_0}^{t_f} \|\mathbf{u}(\mathbf{t})\|^2 \, \mathrm{dt} \tag{26}$$

In discrete time with equal time steps, the cost function for n spacecraft becomes:

$$J(\mathbf{x}, \mathbf{u}) = \sum_{j=1}^{n} \sum_{t_0}^{t_f} \|\mathbf{u}(\mathbf{t})\|^2 \tag{27}$$

The above cost function can further be adapted for non-equal time steps:

$$J(\mathbf{x}, \mathbf{u}) = \sum_{j=1}^{n} \sum_{t_0}^{t_f} \|\mathbf{u}(\mathbf{t})\|^2 \, \Delta t \tag{28}$$

Terminal Cost

A terminal cost function can also be written to penalize (and subsequently, minimize) the error from the current to the desired state. The (discrete) terminal cost function can be expressed as:

$$J(\mathbf{x}, \mathbf{u}) = \sum_{j=1}^{n_d} \sum_{t_0}^{t_f} \|\mathbf{x}(t) - \mathbf{x}_d\|^2 \, \Delta t \tag{29}$$

D. Coulomb's Law

Coulomb's Law describes the forces interacting between n fixed electrically-charged particles. For $j = 1, \ldots, n \neq i$, the electrical force on a particle P_i is inversely proportional to the distances between all other particles P_j and is proportional to the product of the electrical charges q_i and q_j and Coulomb's constant, $k_e = 8.99 \times 10^9 \frac{Nm^2}{C^2}$.

$$\mathbf{F_i} = \sum_{j=1 \neq i}^{n} \frac{k_e q_i q_j}{\left\|\mathbf{r}_{ij}\right\|^2} \tag{30}$$

Note that $\mathbf{r}_{ij}$ is relative position vector pointing from P_i to P_j. It can be easily seen that two like charges will yield a repulsive force and two opposite charges will yield an attractive force. If either or both particles are neutrally charged, then no Coulomb force exists between the particles.

III. Methodology

A. Problem Set-up

In this research, an n-spacecraft system relative to a chief-fixed frame is propagated based on the optimal set of spacecraft charges, $\{c_1(t_i), c_2(t_i), \ldots, c_{n_d}(t_i)\}$, for all time $t \in [t_0, t_f]$. Note that in this research $n = n_d + 1$, where n is the total number of spacecraft (including one neutrally-charged chief spacecraft) and n_d is the number of electrically-charged deputy spacecraft. Consequently, the spacecraft charges produce resultant Coulomb force vectors.

Figure 2 shows an example of a four-spacecraft formation ($n_d = 3$), where the deputy spacecraft are represented as white circles and the chief spacecraft is represented as a black circle for $t \in [t_i, t_{i+1}]$. At time t_i, the Coulomb forces $\mathbf{F_{j,k}}(t)$ for $j, k = 1, \ldots, 3$ on each spacecraft are computed to find a resultant Coulomb force $\mathbf{F_{R,j}}(t_i)$ for the j^{th} spacecraft. A desired state $\mathbf{x}_{d,j}$ for each spacecraft (represented as white stars) is also inputed into the problem. DMS is optionally used to first solve for $\mathbf{u}_j^*(t_i)$, depending on the choice of method. Note that the large black circles (represented by the solid black lines) represent the Debye length radius for each spacecraft. Collision avoidance is not considered in this problem.

Each spacecraft charge state, $c_j(t_i)$ comes from a discrete set of charge states. In order to find the actual charge on the spacecraft, the charge state is multiplied by a constant nominal charge, q_{nom}. Spacecraft charges are modeled as discrete values (as opposed to analog values) and based on a constant q_{nom}, since each spacecraft is assumed to be capable of controlling its own surface charge through onboard feedback control. In reality, the spacecraft is subject to a varying charge plasma environment and surface charge varies over time (i.e. spacecraft charge are analog values). Future work entails modeling the spacecraft charges based on analog values.

The resultant Coulomb force vectors are solved from the spacecraft charge states (using either Method 1 or Method 2). Method 1 (an indirect approach) aims to find the optimal thrust input, $\mathbf{u}_j(t_i)$, and compare that with the resultant Coulomb force vector, $\mathbf{F}_{R,j}(t_i)$ for all deputy spacecraft $j = 1, \ldots, n_d$. In Method 1, the set of resultant Coulomb forces is found such that $\sum_{j=1}^{n_d} \theta_j(t_i)$ is minimized for each time t_i. Here, $\theta_j(t_i)$ is the angle between the vectors $\mathbf{u}_j^*(t_i)$ and $\mathbf{F_{R,j}}(t_i)$. Note that the electrically-charged spacecraft can only produce a limited set of resultant Coulomb forces, while the optimal thrust input can be nearly any direction or magnitude (within the upper and lower thrust input bounds). The set of optimal resultant Coulomb forces for all deputy spacecraft, $\mathbf{F}_{\mathbf{R}}^*(t_i)$, is then input into the relative orbit dynamics in order to propagate the state from $\mathbf{x}_j(t_i)$ to $\mathbf{x}_j(t_{i+1})$ for all deputy spacecraft $j = 1, \ldots, n_d$. The propagated states are represented as dashed white circles. Method 2 (a direct approach) does not solve for an optimal thrust input $\mathbf{u}_j^*(t_i)$, but instead directly solves for the spacecraft charge states $\{c_1(t_i), c_2(t_i), \ldots, c_{n_d}(t_i)\}$ and then computes the resultant Coulomb force vectors.

Note that multiple time steps are required to find $\mathbf{F}_{\mathbf{R}}^*(t_i)$ and solve for the optimal trajectory, depending upon the selection of initial and final conditions. While it is possible for a single Coulomb force input at time t_0 (and no inputs for the remaining time) to produce an optimal trajectory, it is highly unlikely since there are a limited set of resultant Coulomb forces for all n_d spacecraft.

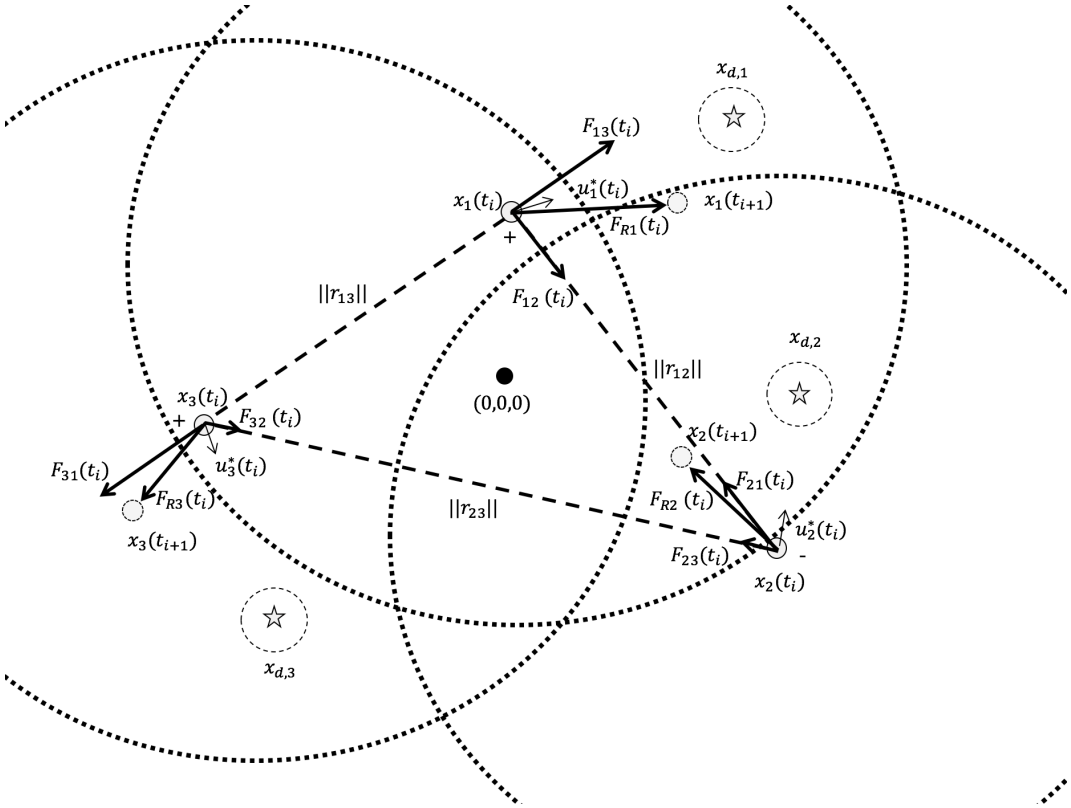

Fig. 2 Problem Set-up. A four-spacecraft system (three deputy spacecraft relative to a chief spacecraft) is propagated based on the optimal set of Coulomb forces for $t \in [t_0, t_f]$ Note that Method 1, in its entirety, indirectly solves for the optimal set of Coulomb forces and charge states by first solving for the optimal thrust input, u_j^*, (Method 1a) and then comparing the result to a set of all possible charge states over all $j = 1, \ldots, n_d$ spacecraft (Method 1b). Method 2 directly solves for the optimal set of charge states over all time steps.

B. Dynamic Environment

1. Assumptions

The following assumptions apply to the n spacecraft formation (note that $n = n_d + 1$):

1) All bodies are considered point masses.
2) All n spacecraft orbit a central body, Earth.
3) All n spacecraft have equal mass.
4) All n spacecraft are capable of controlling surface charge with feedback control.
5) All n_d deputy spacecraft may take one of three charge states $C : \{+, -, 0\}$. The charge state of the chief spacecraft is 0 (i.e. the chief spacecraft is neutrally-charged).
6) Spacecraft charge* is uniformly distributed over each spacecraft and does not decay over the brief period of time.
7) The chief spacecraft is fixed in LVLH frame and positioned at $(0, 0, 0)$.
8) Spacecraft are separated by distances on the order of meters.
9) Spacecraft motions are small compared to the chief orbit radius, $\mathbf{R}_0$
10) Short- and long-term secular orbit effects are ignored.
11) External forces (e.g. solar radiation pressure, third-body effects, atmospheric drag, etc.) are neglected. The only forces acting on the n spacecraft formation are gravity due to Earth and spacecraft Coulomb forces.

The environment is purposefully kept simple in order to efficiently develop and test various algorithms.

*Note that the charge on the j^{th} spacecraft at time t_i is found by multiplying the charge state $c_j(t_i)$ (selected from the set $C_j(t_i) : \{+1, -1, 0\}$) by a constant nominal charge, q_{nom}. For a small satellite, $10^{-7} \leq q_{\text{nom}} \leq 10^{-5}$. q_{nom} is 10^{-6} C in this research.

2. Reference Frame Notation

This research effort aims to propagate the relative position and velocity vector $\mathbf{x}_j(t_i) = \begin{bmatrix} x, & y, & z, & \dot{x}, & \dot{y}, & \dot{z} \end{bmatrix}^T$ forwards in time in a chief-fixed LVLH frame with acting Coulomb forces. The relative spacecraft position vector, $\ell_j(t_i) = [x_j, y_j, z_j]^T$, from the j^{th} deputy spacecraft to the chief spacecraft is formulated in the chief-fixed LVLH frame for $j = 1, \ldots, n_d$:

$$\ell_j(t) = \mathbf{R}_j - \mathbf{R}_0 \tag{31}$$

$$= \begin{bmatrix} x_j + R_0, & y_j, & z_j, \end{bmatrix}^T - \begin{bmatrix} R_0, & 0, & 0 \end{bmatrix}^T \tag{32}$$

$$= \begin{bmatrix} x_j, & y_j, & z_j \end{bmatrix}^T \tag{33}$$

Similarly, the relative velocity vector for the j^{th} spacecraft is defined as the difference between the inertial velocity vectors of the chief spacecraft and j^{th} deputy spacecraft (expressed in LVLH coordinates), for $j = 1, \ldots, n_d$:

$$\dot{\ell}_j(t) = \dot{\mathbf{R}}_j - \dot{\mathbf{R}}_0 \tag{34}$$

$$= \begin{bmatrix} \dot{x}_j + \dot{R}_0, & \dot{y}_j, & \dot{z} \end{bmatrix}^T - \begin{bmatrix} \dot{R}_0, & 0, & 0 \end{bmatrix}^T \tag{35}$$

$$= \begin{bmatrix} \dot{x}_j, & \dot{y}_j, & \dot{z}_j \end{bmatrix}^T \tag{36}$$

Two distinct reference frames are defined, the ECI Frame (denoted as $\mathcal{N}$) and the LVLH Frame (denoted as $\mathcal{L}$):

$$\begin{cases} \mathcal{N} & = \{\text{Earth center-of-mass}, \hat{\mathbf{I}}, \hat{\mathbf{J}}, \hat{\mathbf{K}}\} \\ \mathcal{L} & = \{\text{chief center-of-mass}, \hat{\mathbf{x}}, \hat{\mathbf{y}}, \hat{\mathbf{z}}\} \end{cases}$$

Frame $\mathcal{N}$ is an inertial reference frame. That is, the frame is non-rotating and non-accelerating. In Frame $\mathcal{N}$, $\hat{\mathbf{I}}$ lies in the equatorial plane and points towards the Vernal Equinox, $\hat{\mathbf{K}}$ points in the direction of Earth's angular momentum vector, $\mathbf{h}_E$, and $\hat{\mathbf{J}}$ completes the triad via the right-hand rule. Frame $\mathcal{L}$ is a rotating reference frame. In Frame $\mathcal{L}$, $\hat{\mathbf{x}}$ (radial direction) points along the chief spacecraft radius vector (from the center of Earth), $\mathbf{R}_0$, $\hat{\mathbf{z}}$ (cross-track direction) points in the direction of chief orbit angular momentum vector, $\mathbf{h}_0$, and $\hat{\mathbf{y}}$ (along-track direction) completes the triad via the right-hand rule.

C. Orbit Parameters

Since the CW equations are used, the orbit is assumed to be a circular LEO orbit. The following orbit parameters, $\text{œ} = [a, e, i, \Omega, \omega, f]^T$ are used for an International Space Station (ISS)-like orbit:

$$\begin{aligned} a &= 6671000 \text{ m} \\ e &= 0 \\ i &= 51.3 \text{ deg} \\ \Omega &= 0.0 \text{ deg} \\ \omega &= 0.0 \text{ deg} \\ f &= 0.0 \text{ deg} \end{aligned}$$

D. Method 1: Direct Multiple-Shooting and Resultant Coulomb Force Selection

1. Method 1a: Calculation of Optimal Control Thrust Inputs, $\mathbf{u}_j^*(t_i)$

As previously stated, DMS is a numerical approach for solving a BVP. In Method 1a, DMS is used to first solve for the minimum fuel optimal trajectory of each deputy spacecraft for a randomly selected reconfiguration maneuver *without* Coulomb forces with n_d deputy spacecraft. In a DMS approach, the total time, T, is subdivided into N nodes ($N - 1$ intervals) in which all spacecraft states and control inputs are computed for a given dynamic model. The maneuver

starts from the initial state, $\mathbf{x}_j(t_0)$, and ends at the final state, $\mathbf{x}_j(t_f)$. Through the use of DMS, the goal is to closely match $\mathbf{x}_j(t_f)$ with $\mathbf{x}_{d,j}$ and solve for $\mathbf{u}_j^*(t_i)$ for $i = 0, \ldots, N-1$ and $j = 1, \ldots, n_d$.

Within the simulation environment, the spacecraft states and inputs are computed at 21 uniformly-spaced nodes from time $t_0 = 0$ seconds and $t_f = 100$ seconds. The simulation time of 100 seconds was chosen such that the spacecraft stay in a close formation with separation distances on the order of meters. In most simulated cases with initial relative velocities on the order of 1×10^{-1} m/s or less, all spacecraft are contained within a 20 x 20 x 20 m cube. It is shown that Coulomb forcing is applicable in these specific *close* maneuvers (which currently are not selected to have any specific periodicity). Increasing the simulation time has the inherent effect of propagating spacecraft relative positions to a degree in which the spacecraft are too far apart and Coulomb forcing is no longer beneficial. It is possible to discover periodic relative orbits for deputy spacecraft about a chief spacecraft, but that is not the specific focus of this research. It also may be possible to correct for secular drift using Coulomb forces, but that also is left for future work.

At each node, the CW equations are solved via consecutive iteration over a series of 4 sub-nodes. At each sub-node, the states (of all spacecraft) are computed via an explicit 4th-order Runge-Kutta (RK) approximation. Given a dynamical model of the form $\dot{\mathbf{x}} = f(\mathbf{x}, \mathbf{u}, t)$, the explicit 4th-order RK is evaluated at node i and sub-node j is as follows:

$$k_1 = f(\mathbf{x}_{i,j}, \mathbf{u}_i, t_i) \tag{37}$$

$$k_2 = f(\mathbf{x}_{i,j} + \frac{h}{2} \cdot k_1, \mathbf{u}_i, t_i) \tag{38}$$

$$k_3 = f(\mathbf{x}_{i,j} + \frac{h}{2} \cdot k_2, \mathbf{u}_i, t_i) \tag{39}$$

$$k_4 = f(\mathbf{x}_{i,j} + h \cdot k_3, \mathbf{u}_i, t_i) \tag{40}$$

$$\mathbf{x}_{i,j+1} = \mathbf{x}_{i,j} + \frac{h}{6}(k_1 + 2k_2 + 2k_3 + k_4) \tag{41}$$

In order to solve the two-point BVP and find the optimal thrust inputs, $\mathbf{u}_j^*(t_i)$, MATLAB's **fmincon** is used at each node. **fmincon** inputs the objective function, inequality constraints, initial and final conditions (passed as constraints), and upper and lower boundaries on states and inputs. **fmincon** minimizes the objective function over the given constraints and outputs the optimal states and inputs over all time.

Note that DMS may be applied to an n-spacecraft formation. However, for this research, a four-spacecraft formation is used (i.e. three deputy spacecraft relative to one chief spacecraft).

The following initial conditions are used for deputy spacecraft 1, 2, and 3, respectively:

$$\mathbf{x}_1(t_0) = \mathbf{x}_{0,1} = [1.6305, -3.5328, -2.9946, -0.045372, -0.056649, 0.017657]^T$$
$$\mathbf{x}_2(t_0) = \mathbf{x}_{0,2} = [-3.5806, -1.9233, -0.043103, -0.09828, 0.0086181, -0.021753]^T$$
$$\mathbf{x}_3(t_0) = \mathbf{x}_{0,3} = [0.51562, 1.5102, -4.2894, 0.062217, -0.085625, -0.078863]^T$$

Similarly, the following final (desired) conditions are used for deputy spacecraft 1, 2, and 3, respectively:

$$\mathbf{x}_1(t_f) = \mathbf{x}_{f,1} = [-3.5194, -8.6244, -1.2128, -0.057511, -0.044714, 0.01794]^T$$
$$\mathbf{x}_2(t_f) = \mathbf{x}_{f,1} = [-13.359, 0.073821, -2.2132, -0.097068, 0.031278, -0.021601]^T$$
$$\mathbf{x}_3(t_f) = \mathbf{x}_{f,1} = [5.7427, -7.6966, -12.129, 0.042208, -0.097738, -0.077759]^T$$

The initial and final conditions are randomly chosen such that each spacecraft undergoes a minute maneuver (on the order of meters) for a brief period of time. The initial and final conditions do not imply any periodicity in the relative orbit, but rather show that the algorithms implemented are capable and robust enough to handle a variety of initial and final conditions.

2. Method 1b: Calculation of Spacecraft Resultant Coulomb Forces, $\mathbf{F}_{R,j}(t_i)$

In order to closely resemble the trajectory produced from the optimal thrust inputs, the angle between the optimal thrust input (found in Method 1a) and the optimal resultant Coulomb force vector is minimized. Given n_d deputy

spacecraft, there are k possible charge states for $k = 1, \ldots, 3^{n_d}$ (assuming that a spacecraft can take a positive, negative, or neutral charge). For each case, the resultant Coulomb force vectors, $\mathbf{F}_{R,j}(t_i)$, are calculated via Coulomb's Law for $i = 0, \ldots, N-1$ and $j = 1, \ldots, n_d$. For the j^{th} spacecraft, each resultant force vector produced (from a specific set of charge states) is compared to the optimal thrust input, $\mathbf{u}_j^*(t_i)$ and an angle is found via:

$$\theta_{j,k}(t_i) = \frac{\mathbf{u}_j^*(t_i) \cdot \mathbf{F}_{R,jk}(t_i)}{\left\|\mathbf{u}_j^*(t_i)\right\| \left\|\mathbf{F}_{R,jk}(t_i)\right\|} \tag{42}$$

Note that $\theta_{j,k}(t_i)$ is not included in the cost function of Method 1a. The *set* of Coulomb forces at time t_i is compared to the optimal thrust input $\mathbf{u}(t_i)$ in Method 1b via $\theta_{j,k}(t_i)$. Furthermore, while it may be possible for the optimal thrust input and the optimal resultant Coulomb force vector to align, it is not likely. Recall that the electrically-charged spacecraft can only produce a limited set of resultant Coulomb forces and the optimal thrust input can be any direction or magnitude.

E. Method 2: Optimal Control from Charge States

Method 2 involves formulating an OCP and solving directly for the charge states of each deputy spacecraft, $c_j \in \{+, -, 0\}$, at each instance in time, $t \in [t_0, t_f]$. Note that $c = [c_1, c_2, \ldots, c_j, \ldots c_{n_d}]$ and is the vector of all spacecraft charge states for $j = 1, \ldots, n_d$. Let $\tilde{\mathbf{u}}_j$ be defined as the resultant Coulomb force vector $\mathbf{F}_{R,j}$ for the j^{th} deputy spacecraft. The OCP with constraints becomes:

$$\begin{aligned} \min_{c \in C = \{+,-,0\}} \quad & \underbrace{\sum_{j=1}^{n_d} \frac{1}{2} [\mathbf{x_j}(t_f) - \mathbf{x_{d,j}}]^T [\mathbf{x_j}(t_f) - \mathbf{x_{d,j}}]}_{=\Psi(\mathbf{x_f}, t_f)} \\ \text{subject to} \quad & \dot{\mathbf{x}}_\mathbf{j} = A\mathbf{x_j} + B\tilde{\mathbf{u}}_\mathbf{j}, \text{ for } j = 1, \ldots, n_d, \\ & \mathbf{x_j}(t_0) = \mathbf{x_{j,0}} \text{ for } j = 1, \ldots, n_d. \end{aligned} \tag{43}$$

Note that in this formulation, the Lagrangian $\mathcal{L} = 0$. Let $\tilde{\mathbf{u}} = [\tilde{\mathbf{u}}_1, \tilde{\mathbf{u}}_2, \ldots, \tilde{\mathbf{u}}_{n_d}]^T$ for $j = 1, \ldots, n_d$. Then, the Hamiltonian, $\mathcal{H}$, of the OCP is defined as:

$$\mathcal{H} = \underbrace{\mathcal{L}}_{=0} + \boldsymbol{\lambda}^T \mathbf{f} = \boldsymbol{\lambda}^T (A\mathbf{x} + B\tilde{\mathbf{u}}) \tag{44}$$

The FONC for Optimality can be derived next. First, application of Pontryagin's Maximum Principle (PMP) yields a constraint on $\tilde{\mathbf{u}}^*$:

$$\tilde{\mathbf{u}}^* = \underset{c \in C = \{+,-,0\}}{\operatorname{argmin}} \mathcal{H} = \underset{c \in C = \{+,-,0\}}{\operatorname{argmin}} \boldsymbol{\lambda}^T B\tilde{\mathbf{u}} \tag{45}$$

Note that $\tilde{\mathbf{u}}_j = F(\mathbf{x}, \mathbf{c}) = \sum_{j=1 \neq i}^{n_d} k_e \frac{q_j q_i}{d_{ij}^2}$.

The dynamics of $\boldsymbol{\lambda}$ can be found:

$$\dot{\boldsymbol{\lambda}} = -\frac{\partial \mathcal{H}^T}{\partial \mathbf{x}} = -\left[\boldsymbol{\lambda}^T A\right]^T = -A^T \boldsymbol{\lambda} \tag{46}$$

The above differential equation can be solved and expressed as a function of time, t:

$$\boldsymbol{\lambda}(t) = e^{-A^T t} \boldsymbol{\lambda}(t_0) \tag{47}$$

Next, the terminal condition on $\boldsymbol{\lambda}$ at time $t = t_f$ can be solved:

$$\boldsymbol{\lambda}(t_f) = \frac{\partial \Psi^T}{\partial \mathbf{x}}(\mathbf{x}(t_f), t_f) = \frac{\partial}{\partial \mathbf{x}} \left[\sum_{j=1}^{n_d} \frac{1}{2} \{\mathbf{x}_j(t_f) - \mathbf{x}_{\mathbf{d}j}\}^T \{\mathbf{x}_j(t_f) - \mathbf{x}_{\mathbf{d}j}\} \right]^T = \mathbf{x}(t_f) - \mathbf{x_d} \tag{48}$$

Equations (43),(45), (46), and (48) now provide a sufficient amount of information to describe and solve the OCP. In order to solve the OCP, a steepest descent approach is applied through successive iterations $k = 0, \ldots, k_{max}$ to a function $G(\boldsymbol{\lambda}(t_0)) = \left[\boldsymbol{\lambda}(t_f) - \mathbf{x}(t_f) + \mathbf{x}_d\right]^T \left[\boldsymbol{\lambda}(t_f) - \mathbf{x}(t_f) + \mathbf{x}_d\right]$.

The algorithm used is described below:

1) Set $k = 0$ and tol = 1×10^{-2}.
2) Guess $\boldsymbol{\lambda}_k(t_i)$.
3) Find $\tilde{\mathbf{u}}_k^*(t_i) = \text{argmin}[\boldsymbol{\lambda}_k^T B \tilde{\mathbf{u}}_k(t_i)]$. The solution to $\tilde{\mathbf{u}}_k^*(t_i)$ occurs when $\boldsymbol{\lambda}_k^T B \cdot \tilde{\mathbf{u}}_k(t_i)$ is minimized. $\tilde{\mathbf{u}}_k(t_i)$ is evaluated for all 3^{n_d} charge state combinations.
4) With $\mathbf{x}(t_i) = \mathbf{x}_0$, propagate the state forward to $\mathbf{x}_k(t_1)$ with $\dot{\mathbf{x}} = A\mathbf{x}_0 + \mathrm{B}\tilde{\mathbf{u}}_k^*(t_i)$.
5) With $\boldsymbol{\lambda}_k(t_i)$, propagate the co-state forward to $\boldsymbol{\lambda}_k(t_1)$ with $\dot{\boldsymbol{\lambda}} = -A^T \boldsymbol{\lambda}_k(t_i)$
6) Repeat step 3 - 5 for $t \in \left[t_0, t_f\right]$ with time-step dt. Obtain $\boldsymbol{\lambda}_k(t_f)$ and $\mathbf{x}_k(t_f)$.
7) Evaluate $G_k = \left[\boldsymbol{\lambda}_k(t_f) - \mathbf{x}_k(t_f) + \mathbf{x_d}\right]^T \left[\boldsymbol{\lambda}_k(t_f) - \mathbf{x}_k(t_f) + \mathbf{x_d}\right]$.
8) If $G_k \leq$ tol = 1×10^{-2}, stop. If $G_k >$ tol = 1×10^{-2}, take a small step to find G_{k+1}. Evaluate ∇G_k via test-shooting or Broyden-Fletcher-Goldfarb-Shanno (BFGS) via **fsolve**.
9) Find $\boldsymbol{\lambda}_{k+1}(t_i) = \boldsymbol{\lambda}_k(t_i) - \alpha \nabla G_k$. Let $\alpha = 1$.
10) Repeat steps 3 - 9 until $G_k \leq$ tol = 1×10^{-2} or $k > k_{max}$.

The outputs of the algorithm for $t \in [t_0, t_f]$ are: $\tilde{\mathbf{u}}_j^*$, $\mathbf{x}_j$, and $\boldsymbol{\lambda}_j$ for $j = 1, \ldots, n_d$.

IV. Results

A. Method 1

1. Method 1a: Optimal Thrust Inputs

DMS is used to find the states, inputs, and charge states for the minimum fuel two-point BVP. The results shown represent DMS with $N = 21$ nodes and $T = 100$ seconds. Three deputy spacecraft are propagated with the chief fixed at the center of the LVLH frame. It is possible to increase N at the expense of computation time.

Three deputy spacecraft trajectories are represented in Figure 3 as colored lines about a chief, denoted as a black X. The initial and final position of each deputy spacecraft are represented with a green square and a red triangle, respectively. The desired final states are indicated by the red X's. The black arrows represent the calculated thrust inputs at each node. The optimal minimum fuel trajectories enable each deputy spacecraft to reach their desired final state with minimal error. The written code also specifies that spacecraft cannot use Coulomb charging if they are outside the Debye length (30 m), although this condition does not occur during the simulation.

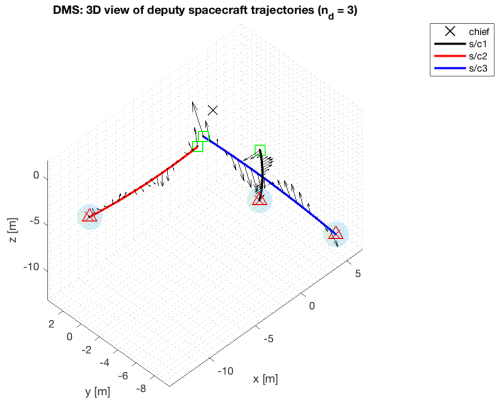

(a) Method 1a: 3-dimensional view

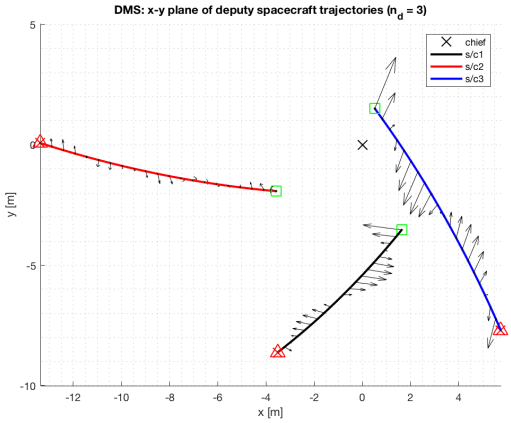

(b) Method 1a: XY plane

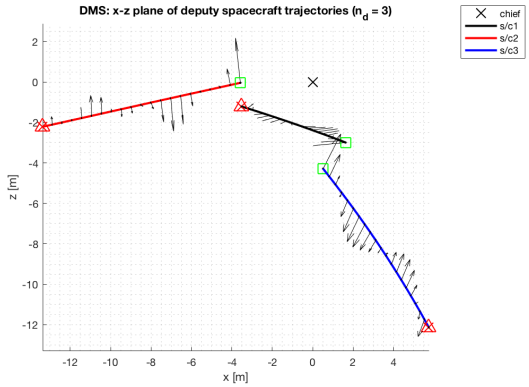

(c) Method 1a: XZ plane

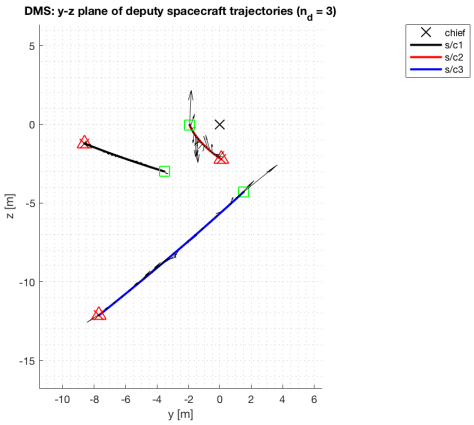

(d) Method 1a: YZ plane

Fig. 3 Method 1a: Four-spacecraft reconfiguration maneuver with optimal thrust inputs, $\mathbf{u}^*$.

Figure 4 shows the control inputs $\mathbf{u}^*$ for the four-spacecraft reconfiguration maneuver. Similarly, Figure 5 shows the relative states for the four-spacecraft reconfiguration maneuver. Convergence to zero in Figure 5 indicates that the deputy spacecraft move to their desired states by the end of the simulation. It is important to note that the control inputs solved via DMS are the optimal thrust inputs that could be produced by a spacecraft propulsion system in order to satisfy the conditions of the two-point BVP. At this point, Coulomb forces have not been introduced to the problem yet. The subsequent section introduces the minimization of the angle formed between the optimal thrust vector and the optimal resultant Coulomb force vector. With active control (based on minimum fuel), the results of Method 1a show the best-case scenario for the reconfiguration maneuver. Method 1b and Method 2 introduce Coulomb forces, which restrict the selection of all control inputs.

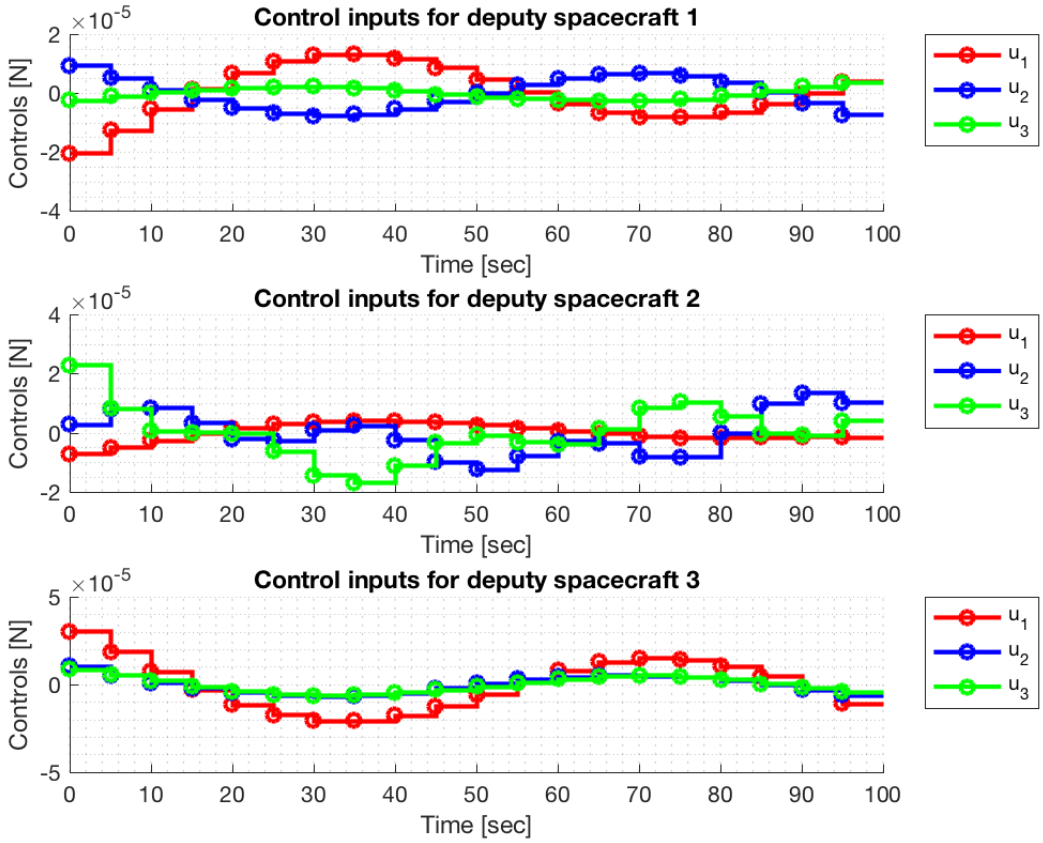

Fig. 4 Method 1a: Optimal control thrust inputs. Each component of the optimal control thrust input for each deputy spacecraft is represented in the LVLH frame.

Figure 5 shows the relative states for each deputy spacecraft. The states are approximately linear due to the short time duration of the simulation (100 sec) compared to the orbit period.

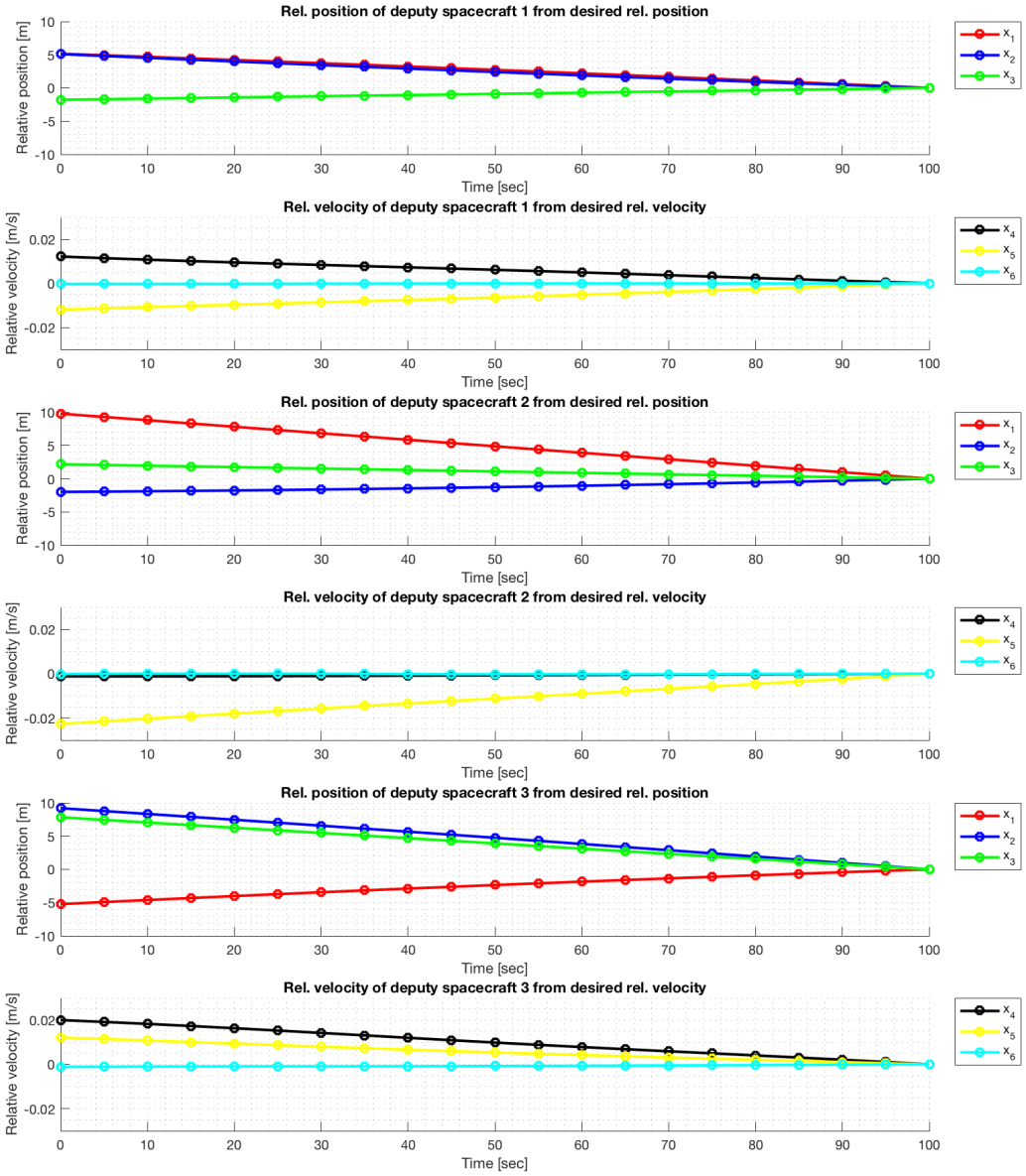

Fig. 5 Method 1a: Relative states from optimal thrust inputs.

2. Method 1b: Resultant Coulomb Forces

The optimal resultant Coulomb force is found in Method 1b such that $\sum_{i=0}^{N-1} \sum_{j=1}^{n_d} \theta_{j,k}(t_i)$ is minimized, where $i = 0, \ldots, N-1$, $j = 1, \ldots, n_d$, and $k = 1, \ldots, 3^{n_d}$. k denotes the iteration number over the set of all possible Coulomb charge states for n_d spacecraft and may vary between time steps.

Figure 6 shows the trajectories of each deputy spacecraft using Method 1b. Since there is a limited set of possible resultant Coulomb forces, the relative position error between actual and desired final states is significantly larger. Furthermore, since the Coulomb forces are selected such that the angle between $\mathbf{u}_j^*$ and $F_{R,j}^*$ is minimized for $j = 1, \ldots, n_d$, the spacecraft easily deviate from the optimal minimum fuel trajectory. The trajectories do not closely follow those shown in Figure 3.

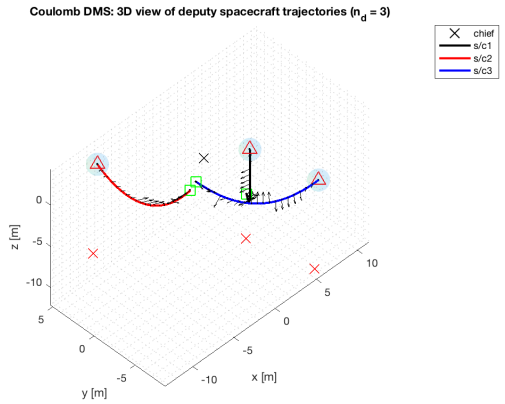

(a) Method 1b: 3-dimensional view

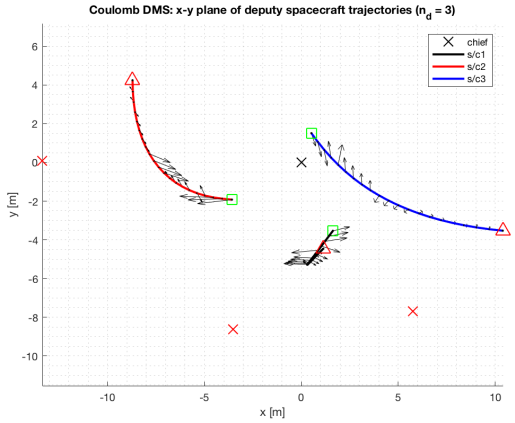

(b) Method 1b: XY plane

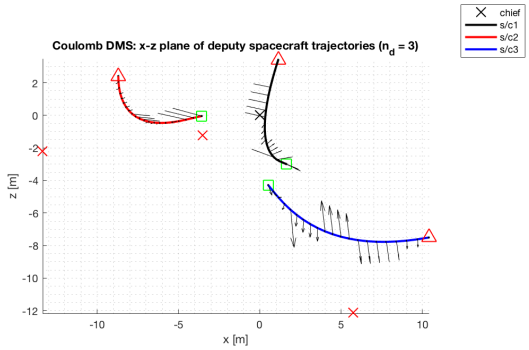

(c) Method 1b: XZ plane

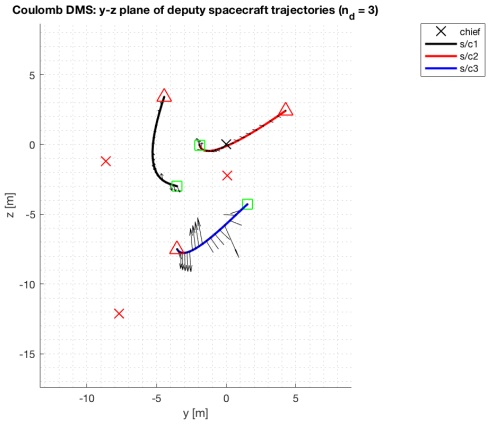

(d) Method 1b: YZ plane

Fig. 6 Method 1b: Four-spacecraft reconfiguration maneuver with calculated Coulomb forces, $\mathbf{F}_R^*$.

The control inputs and states for the 3-spacecraft reconfiguration maneuver with Coulomb forces are shown in Figures 7 and 8. The inputs are more chaotic in nature that those in Figure 4, since the algorithm attempts to match up Coulomb forces with the optimal thrust input.

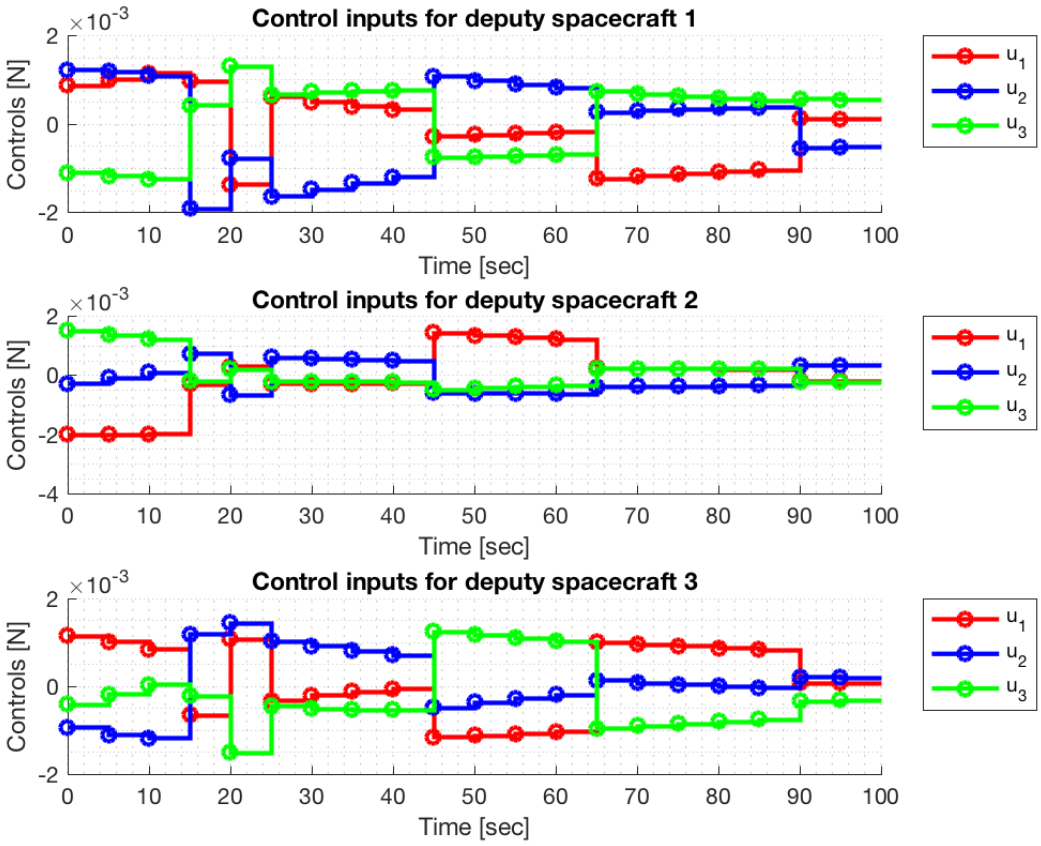

Fig. 7 Method 1b: Control inputs.

Figure 8 shows the relative states of the deputy spacecraft using Method 1b. In general, the relative states over all times do not resemble those shown in Figure 5 (Method 1a). Once the Coulomb force state deviates from the optimal trajectory state, the angle minimization method breaks down.

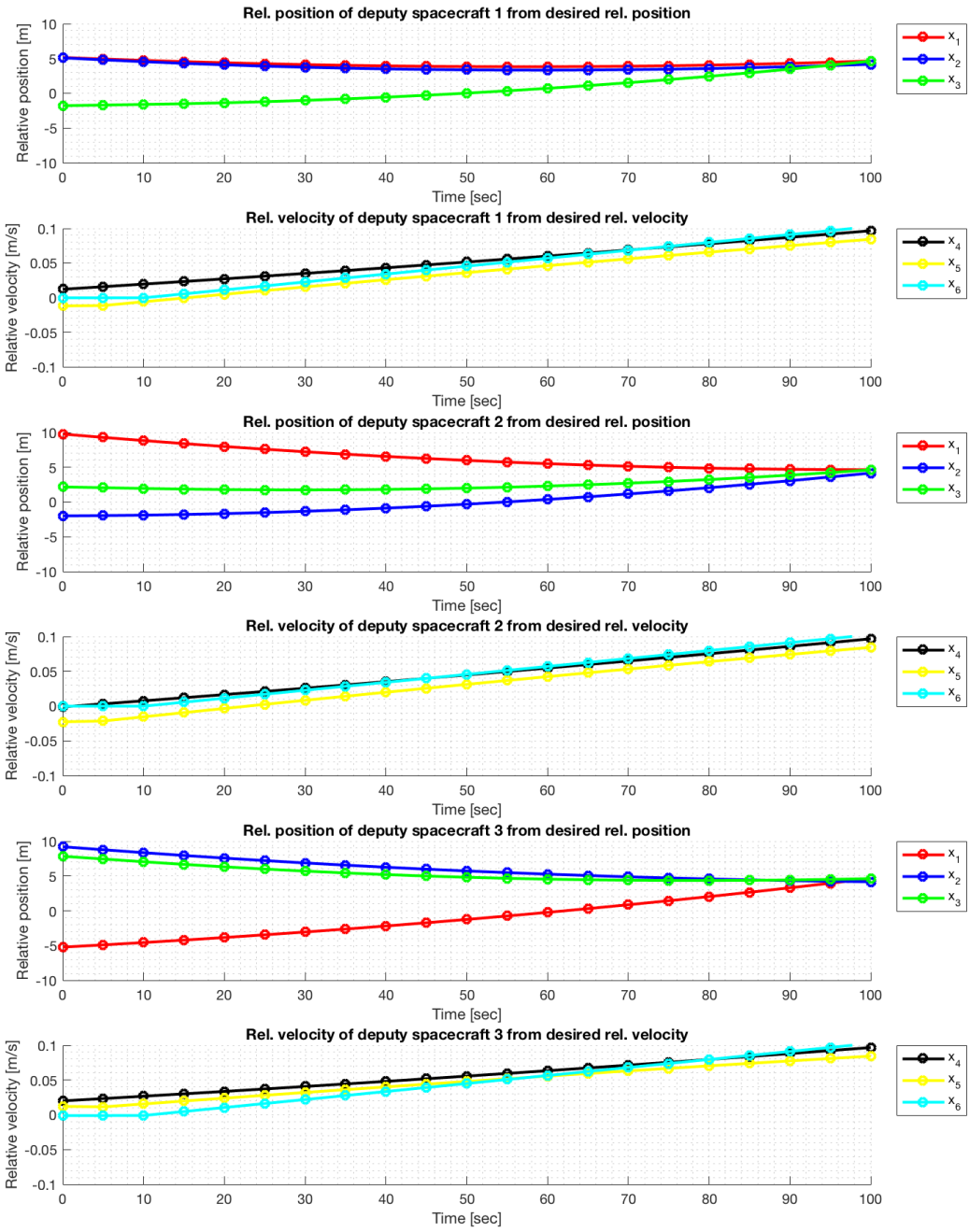

Fig. 8 Method 1b: Relative states.

The spacecraft charges $c_j(t_i)$ are shown in Figure 9 for $j = 1, \ldots, n_d$ and $i = 0, \ldots, N-1$. The charges dynamically change sign, producing either repulsive or attractive forces between pairs of spacecraft.

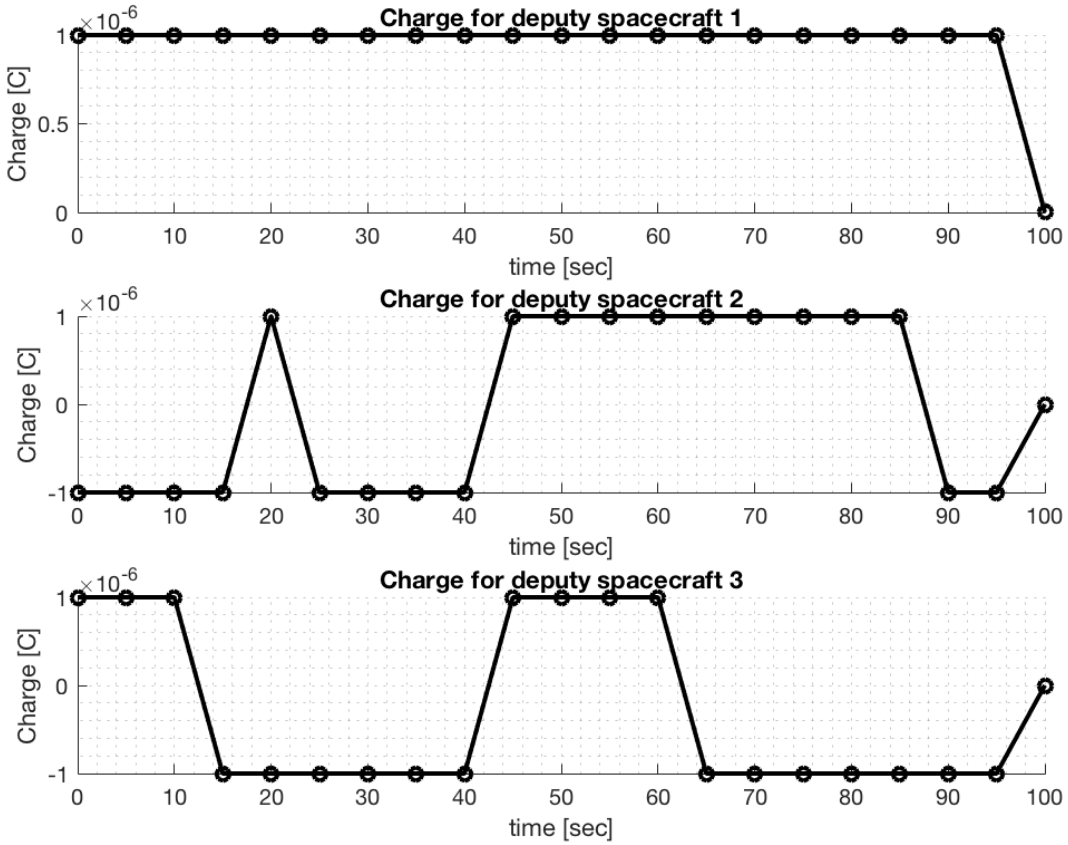

Fig. 9 Method 1b: Spacecraft Charges.

B. Method 2

Method 2 aims to solve the OCP iteratively by finding the corresponding states and co-states corresponding to the condition $\nabla G_k = 0$, where $G_k = [\boldsymbol{\lambda}_k(t_f) - \mathbf{x}_k(t_f) + \mathbf{x}_d]^T [\boldsymbol{\lambda}_k(t_f) - \mathbf{x}_k(t_f) + \mathbf{x}_d] > 0$ and k is the iteration number. Note that G_k is purposefully a positive-definite, convex function. $\nabla G_k = 0$ occurs when the global minimum is found of the convex function G_k. In practice, $G_k <$ tol is implemented, where $10^{-6} \leq$ tol ≤ 1, depending upon the size of n_d.

The optimal Coulomb forces are forces are found from the optimal set of Coulomb charges at each instance in time. The forces are inputs into the dynamical equations that also satisfy the above constraint. The full algorithm is illustrated in Section III.

As shown in Figure 10, Method 2 optimally controls the states of all deputy spacecraft with minimal error. Method 2 closely resembles the results found from Figure 3 (Method 1a) and is clearly superior than the results shown in Figure 6 (Method 1b) in terms of final relative state vector error.

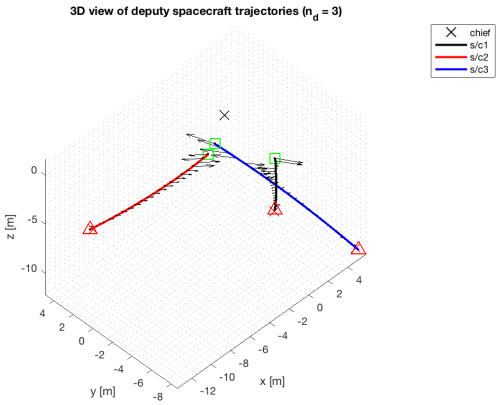

(a) Method 2: 3-dimensional view

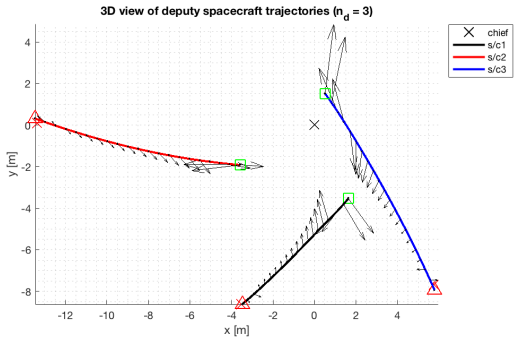

(b) Method 2: XY plane

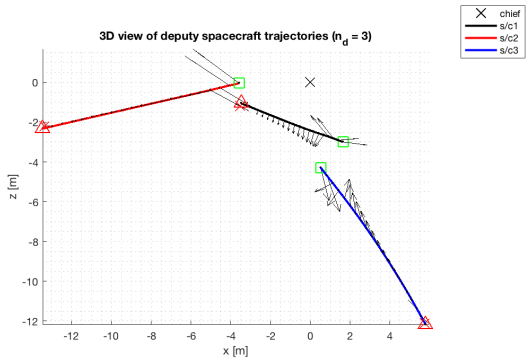

(c) Method 2: XZ plane

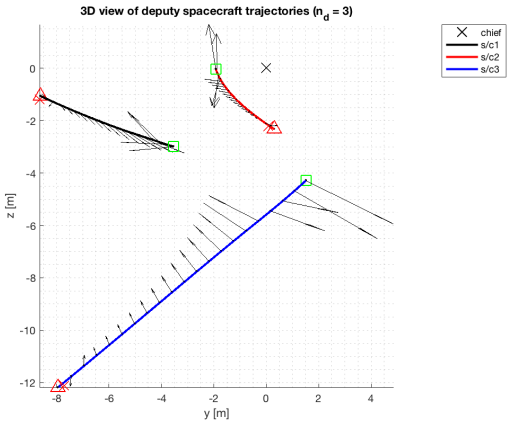

(d) Method 2: YZ plane

Fig. 10 Method 2: Four-spacecraft reconfiguration maneuver with optimal Coulomb forces, F_R^*.

Figure 11 shows that the Coulomb force magnitudes (in each LVLH direction) naturally decay as the deputy spacecraft become farther apart over time. This result aligns with Figure 4. As the time step h decreases, the control inputs become smoother.

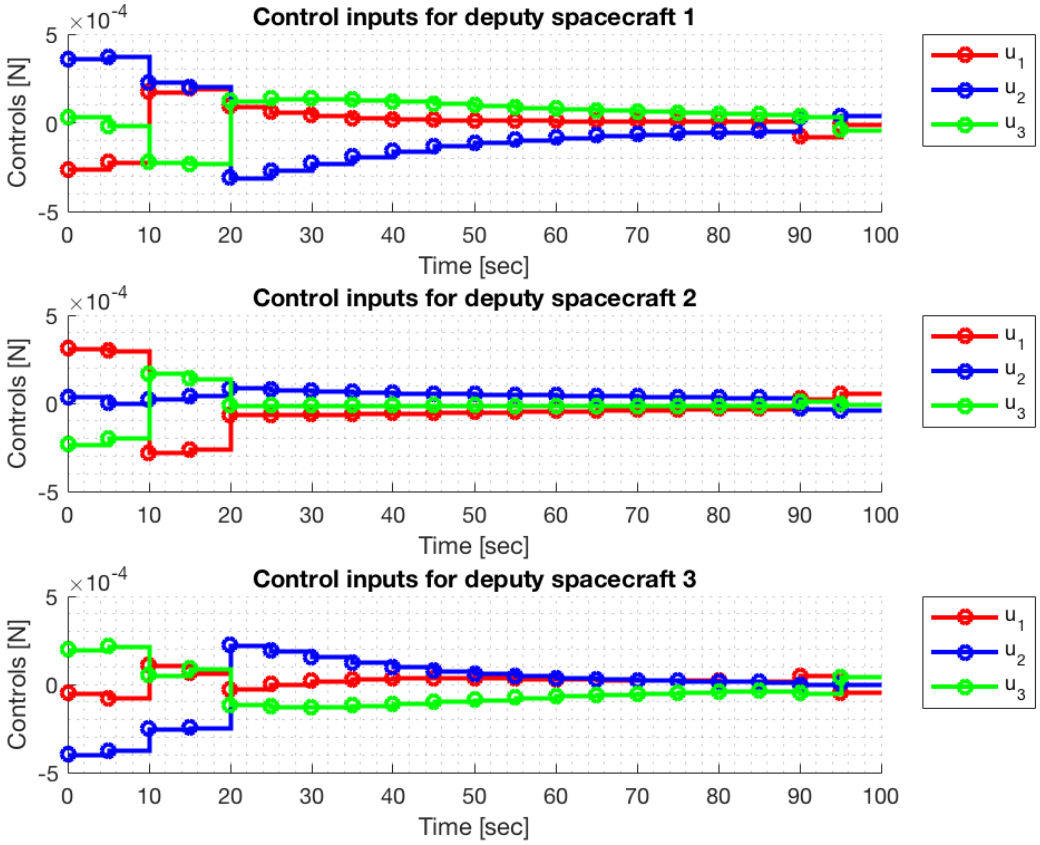

Fig. 11 Method 2: Control inputs.

Figure 12 shows that the relative states from Method 2 generally align with those shown in Figure 5 and minimize the final relative state vector error.

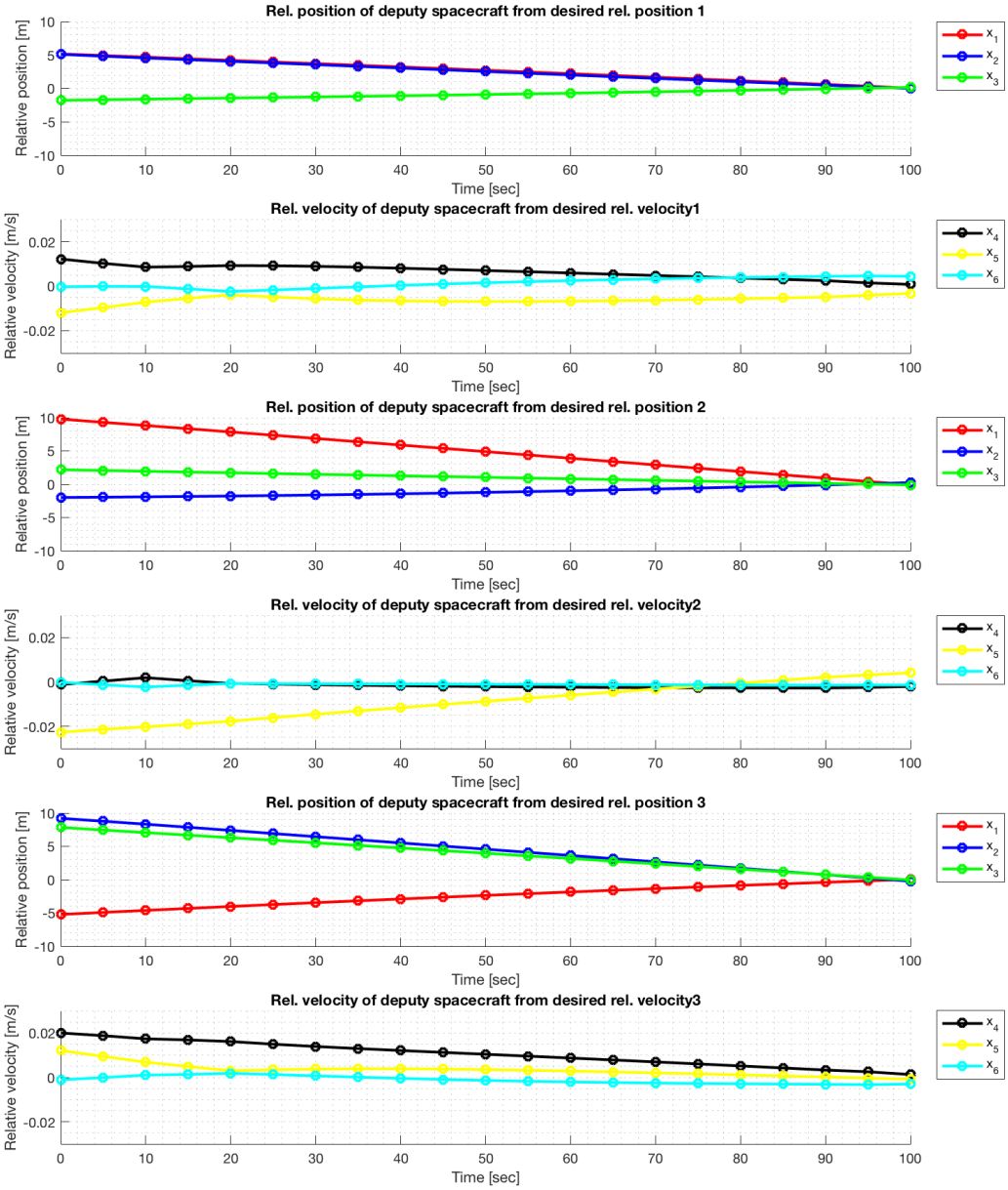

Fig. 12 Method 2: Relative states.

The spacecraft charge states in Figure 13 switch fewer times than in Method 1. In several tried examples with varying initial and final conditions, a spacecraft became neutrally charged only when the spacecraft was extremely close to its final desired state (< 1 m). Method 2 seeks to actively control the spacecraft and, thus, it is logical that each spacecraft must be charged positively or negatively.

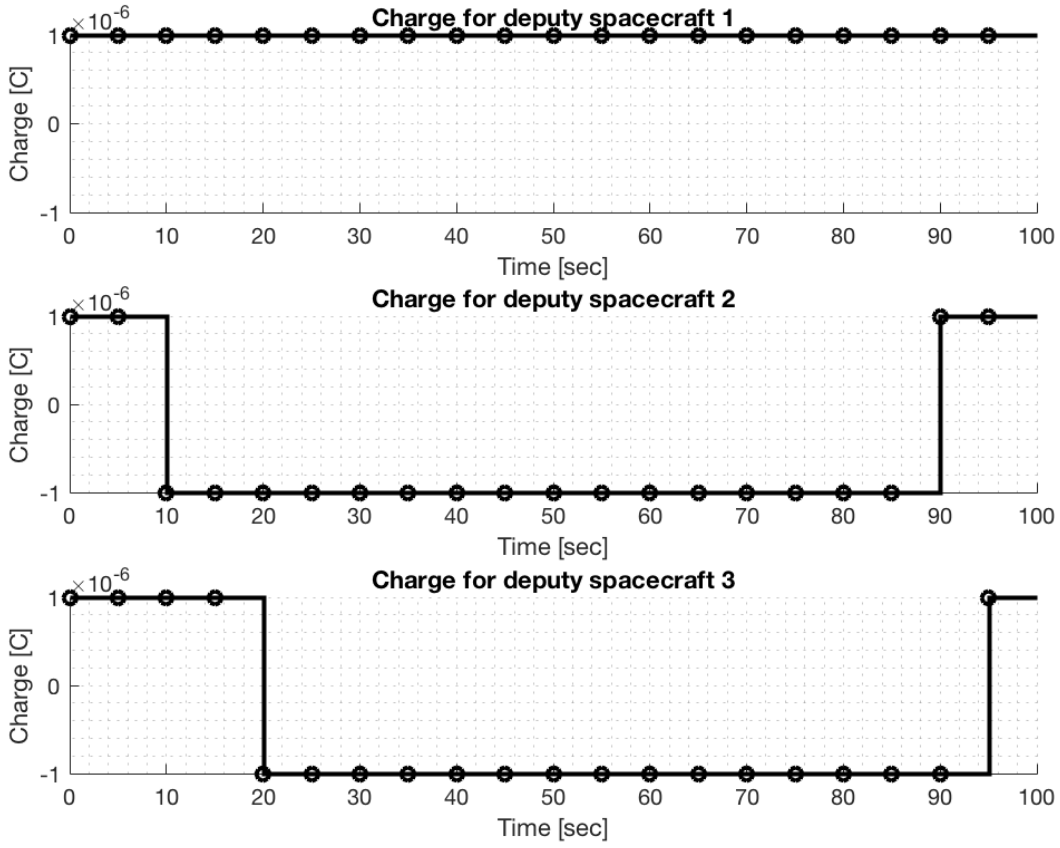

Fig. 13 Method 2: Spacecraft Charges.

Method 2 is vastly superior to Method 1b in terms of final state vector error for any n_d. However, the minimum fuel trajectory (Method 1a) is slightly better than Method 2 (optimal control using Coulomb forces). Method 1a and Method 2 both show a monotonically decreasing curve, but Method 1a outperforms Method 2 at the last time step. This is due to the fact that Method 1a is calculated via DMS and maintains strict equality constraints, while Method 2 finds an optimal Coulomb force trajectory from a function G_k based on the co-state at t_f, the state at t_f, and desired final state. Method 2 does not always converge to the true desired state, since the terminal cost is not a hard constraint. Lastly, the computed optimal trajectories in Method 2 are sensitive to an initial co-state guess of $\boldsymbol{\lambda}_{0,0}$.

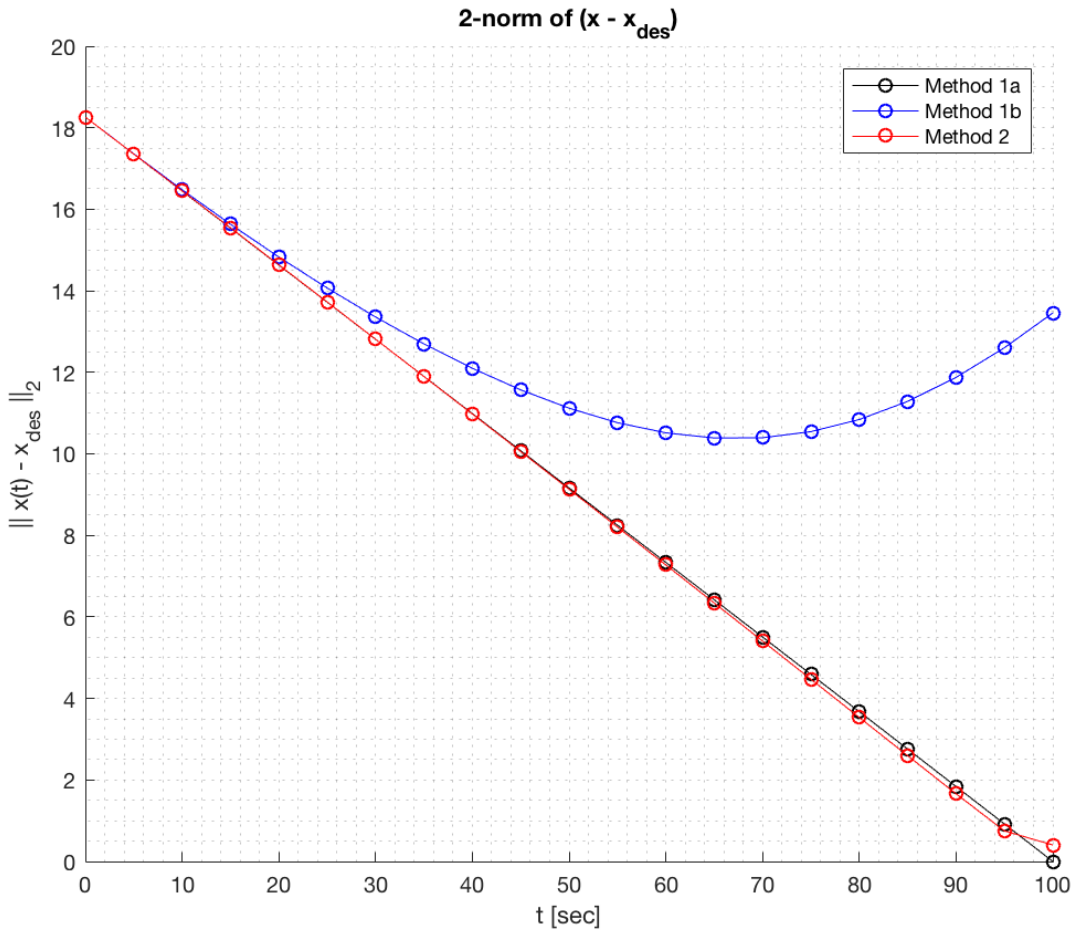

Fig. 14 **State vector relative position error of Methods 1a, 1b, and 2 as a function of time: The relative position from the desired final position of three deputy spacecraft are plotted.**

Figure 15 shows that the magnitude of ∇G_k tends to zero and G_k tends to a minimum as k increases. This is expected behavior since G_k is a formulated as a quadratic convex function and has a global minimum. ∇G_k does not reach true zero, since the algorithm breaks the while loop early once all spacecraft are within tolerance of their final desired states. However, in theory, the true global minimum of G_k occurs when $\nabla G_k = 0$.

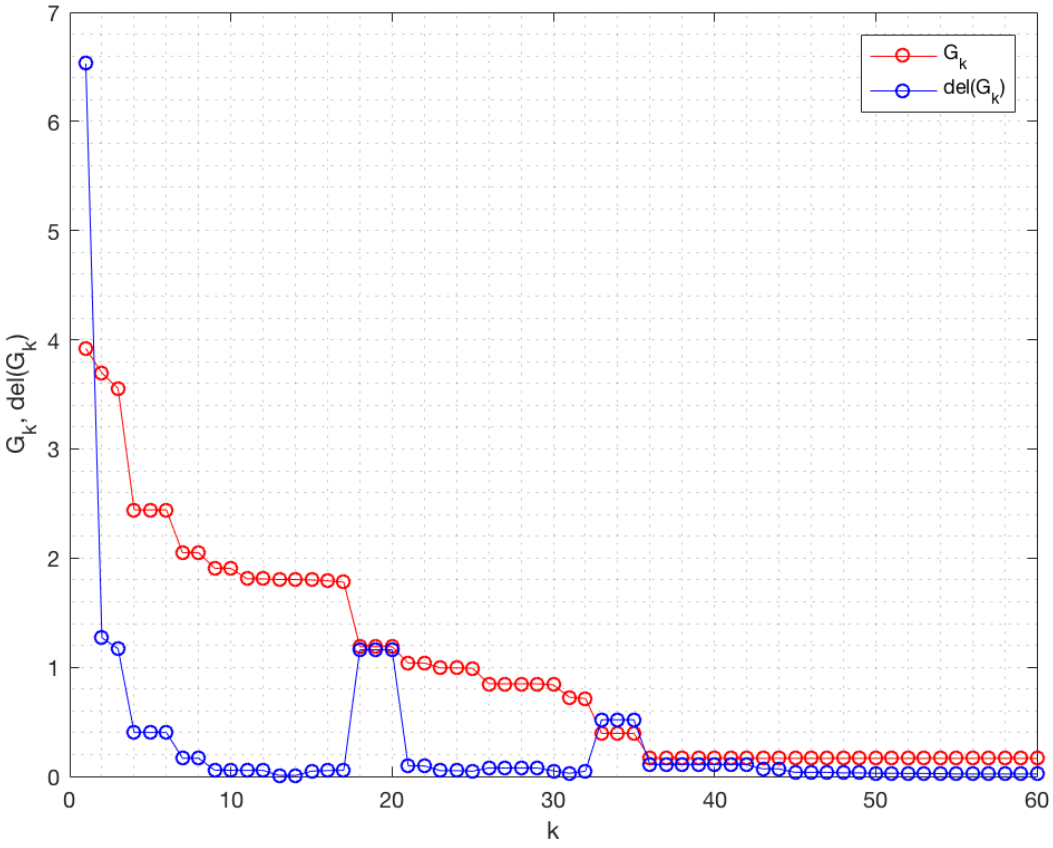

Fig. 15 Method 2: Gradient of G_k and G_k from fsolve. ∇G_k tends to 0, satisfying the first-order necessary condition for optimality. G_k is a convex function and is calculated upon successive iterations. Upon each iteration, the value of G_k decreases until a global minimum is found.

C. Comparison

The state vector error and computational times are shown for Methods 1 and 2 as N is increased. Furthermore, Methods 1 and 2 are compared for increasing number of deputy spacecraft, n_d.

While the optimal trajectory computation (Method 1a) produces minimal error (rounded to zero), the Coulomb force based calculation and angle minimization (Method 1b) produces significant error in terms of final state vector (Figure 16). Furthermore, DMS is shown to take an increasing amount of time without significant improvement.

Effect of Increasing N for Method 1 (n_d = 3, t = 100 s)				
N	‖x*(t_f) - xd‖ *(Method 1a)*	‖x_C(t_f) - xd‖ *(Method 1b)*	*computational time [sec]*	*total iterations [-]*
11	0	11.88	37.1	440
21	0	13.46	247.92	796
31	0	13.35	590.52	883

Fig. 16 Method 1: Results.

Figure 17 that final state vector error (Method 2) approaches a minimum as N is increased. Computational time is relatively constant as **fsolve** sees G_k as a black-box function with input $\boldsymbol{\lambda}_{0,0}$. **fsolve** outputs the optimal choice of $\boldsymbol{\lambda}_{0,0}$ needed to minimize G_k. $\boldsymbol{\lambda}_{0,0}$ is then used as the " best guess " to compute the state and control input dynamics fully.

Effect of Increasing N for Method 2 (n_d = 3, t = 100 s, λ_0 fixed)				
N	‖x(t) - xd‖	*computational time [sec]*	*total iterations [-]*	*min(G_k)*
11	0.84	243.07	55	0.47231
21	0.73	265.47	57	0.472309
101	0.68	235.45	55	0.47231
1001	0.66	231.63	55	0.47231
10001	0.66	258.02	55	0.47231

Fig. 17 Method 2: Results.

Figure 18 compares relative state vector error and computational time for Method 1b and Method 2. Method 2 is superior for each criteria. Note that larger relative position state vector errors are seen as $n_d \geq 4$. It is not recommended to exceed $n_d = 3$ when using Coulomb forces for short duration reconfiguration maneuvers.

Comparison of Method 1b and Method 2 (N = 21, t = 100 s, λ_0 not fixed)				
n_d, n	*‖ x(t) - x_d ‖*		*computational time [sec]*	
	Method 1b	*Method 2*	*Method 1b*	*Method 2*
1, 2	0.00	0.00	236.51	0.72
2, 3	13.25	0.14	454.66	15.83
3, 4	13.46	0.41	743.76	79.5
4, 5	25.72	11.96	985.16	273.71

Fig. 18 Comparison of Methods 1b and 2.

V. Conclusion

It is evident that Method 2 is superior to Method 1b in terms of overall performance. It is logical that Method 2 provides superior results to Method 1b, since it formulated directly from the standpoint of an OCP. While both methods compute the Coulomb force trajectory for n_d deputy spacecraft in the LVLH frame (given the same initial conditions), the final state vector error (from the desired final state vector) differs significantly by an order of magnitude. Unfortunately, Method 1b does not provide a useful or practical contribution to relative position control for spacecraft reconfiguration maneuvers via Coulomb forces. Basing the choice of Coulomb resultant forces (and, thus, spacecraft charge states) on only one calculation of the entire optimal trajectory fails once the spacecraft position becomes too far from the optimal trajectory at time t_i. It is possible that Method 1b may be adapted using model predictive control, however. For each t_i, the optimal trajectory may be re-calculated and the angle minimization technique may be applied for each t_i. This method is left for future work.

In this research, an optimal method of Coulomb force control (Method 2) was developed and tested. It is shown that

the minimum fuel optimal trajectory of Method 1a closely resembles the trajectory of Method 2. While Method 2 does not have the accuracy of Method 1a, this is only due to the restrictions from a Coulomb force based propagation. The OCP formulation yields the optimal charge states of each spacecraft for any given trajectory (assuming all convergence criteria are met). To further generalize Method 2, note that Method 2 increases in accuracy and approaches a minimum final state vector error as the step size is decreased (or N is increased). As $N \to \infty$, the discretized numerical simulation matches that of a continuous time OCP.

As the total number of deputy spacecraft increases, it is seen that Method 2 increases in state vector error. Method 2 works best for $n_d \leq 3$.

The output of Method 2 is also sensitive to the choice of the initial co-state guess $\boldsymbol{\lambda}_{0,0}$. Further refinement of $\boldsymbol{\lambda}_{0,0}$ may yield better results. Furthermore, increasing the number of iterations may enable ∇G_k to further tend to zero and find a better minimum of the convex function G_k. Tolerances implemented within the code to calculate the k^{th} iteration of $\boldsymbol{\lambda}_{0,k}$ may also be refined further. In this research, **fsolve** was used to minimize G_k. ∇G_k is solved with BFGS inside the function. This method of solving for ∇G_k find the optimal point faster and is more accurate than a method such as test-shooting.

Method 2 is also significantly faster than Method 1 in terms of computational time. Recall that Method 1 is based on DMS and rigorously calculates the dynamics at each of the N nodes over M sub-nodes. These numbers were purposefully low ($N \leq 40, M \leq 5$) for efficient computing. Increasing these numbers adds several minutes - or even hours - to the total computational time. Method 2, however, is simply a minimization problem over a black-box function $G_k(\boldsymbol{\lambda}_{0,0})$ and is relatively easy to efficiently compute.

For both Methods 1 and 2, the computations suffer from the curse of dimensionality. The optimal set of resultant Coulomb forces is calculated from the set of all possible resultant Coulomb forces. The size of set is 3^{n_d}, so keeping n_d relatively low ($n_d \leq 3$) is desired.

The assumptions made in this effort may be adapted in the future. Recall that the spacecraft charge states were assumed to be positive, negative, or neutral and the spacecraft charge was neutral. In practice, charge is not uniform and gradually diminishes over time. These effects may slightly vary the final trajectory for Method 2, but are not expected to pose any significant differences in the computed trajectory. Furthermore, a circular orbit was chosen so the CW equations could be applied. While other intensive LVLH frame dynamics were studied, they were not implemented fully due to computational time. Updating the dynamics to extend to all types of orbits of varying eccentricity is a future task to complete.

References

[1] Manu, S., "SBIR/STTR," , 2018. URL `https://sbir.gsfc.nasa.gov/solicit/59380/detail?data=ch9&s=59356&topic=59819`.

[2] Gill, E., et al., "Formation Flying within a constellation of nano-satellites: The QB50 mission," *Acta Astronautica*, Vol. 82, 2013, pp. 110–117.

[3] Chen, Q., et al., "Virtual Spring-Dampter Mesh-Based Formation Control for Spacecraft Swarms in Potential Fields," *Journal of Guidance, Control, and Dynamics*, Vol. 38, No. 3, 2015, pp. 539–546.

[4] Thakur, D., et al., "Spacecraft Swarm Finite-Thrust Cooperative Control for Common Orbit Convergence," *Journal of Guidance, Control, and Dynamics*, Vol. 38, No. 3, 2015, pp. 478–488.

[5] King, L., et al., "Study of Interspacecraft Coulomb Forces and Implications for Formation Flying," *Journal of Propulsion and Power*, Vol. 19, No. 3, 2003, pp. 497–505.

[6] Mesbahi, M., and Hadaegh, F., "Formation Flying Control of Multiple Spacecraft via Graphs, Matrix Inequalities, and Switching," *Journal of Guidance, Control, and Dynamics*, Vol. 24, No. 2, 2001, pp. 369–377.

[7] Morgan, D., and Chung, S., "Spacecraft Swarm Guidance Using a Sequence of Decentralized Convex Optimizations," *AIAA/AAS Astrodynamics Specialist Conference*, 2012.

[8] Morgan, D., and Chung, S., "Swarm Assignment and Trajectory Optimization Using Variable-Swarm, Distributed Auction Assignment and Model Predictive Control," *AIAA SciTech Forum*, 2015.

[9] Lee, K., and Singh, S., "Attractive Manifold-Based Noncertainty-Equivalence Adaptive Spacecraft Formation Flying Using Output Feedback," *AIAA SciTech Forum*, 2018.

[10] Prince, E., and Cobb, R., "Optimal Guidance for Relative Teardrops with Lighting and Collision Constraints," *AIAA SciTech Forum*, 2018.

[11] Tahir, A., and Narang-Siddarth, A., "Constructive Nonlinear Approach to Coulomb Formation Control," *AIAA SciTech Forum*, 2018.

[12] Garcia, E., et al., "Decentralized Event-Triggered Consensus of Autonomous Agents over Unreliable Communication Networks," *AIAA SciTech Forum*, 2018.

[13] Lubberstedt, H., et al., "Novel Satellite Constellation Maintenance Strategy for Low Earth Orbiting Missions Exemplified for Swarm," *IAC*, 2005.

[14] King, L., et al., "Spacecraft Formation-flying using Inter-vehicle Coulomb Forces," *NASA Institute for Advanced Concepts*, 2002.

[15] Ren, W., et al., "Decentralized Scheme for Spacecraft Formation Flying via the Virtual Structure Approach," *Journal of Guidance, Control, and Dynamics*, 2004.

[16] Curtis, S., et al., "Use of Swarm Intelligence in Spacecraft Constellations for the Resource Exploration of the Asteroid Belt," *Third International Workshop on Satellite Constellations and Formation Flying*, 2003.

[17] Morgan, D., and Chung, S., "Swarm-Keeping Strategies for Spacecraft Under J2 and Atmospheric Drag Perturbations," *Journal of Guidance, Control, and Dynamics*, 2012.

[18] Morgan, D., et al., "Model Predictive Control of Swarms of Spacecraft Using Sequential Convex Programming," *Journal of Guidance, Control, and Dynamics*, 2014.

[19] Jeong, D., and Lee, K., "Dispersion and Line Formation in Artificial Swarm Intelligence," *Collective Intelligence*, 2014, pp. 1–4.

[20] Folta, D., et al., "NASA's Autonomous Formation Flying Technology Demonstration, Earth Observing-1 (EO-1)," *International Symposium: Formation Flying Missions and Technology*, Vol. 72, No. 8, 1967, pp. 994–997.

[21] Alfriend, K., et al., *Spacecraft Formation Flying*, 1st ed., Elsevier, 2010.

[22] Schaub, H., et al., "Spacecraft Formation Flying Control using Mean Orbit Elements," *Journal of the Astronautical Sciences*, Vol. 48, No. 1, 2000, pp. 69–87.

[23] Lee, D., et al., "Formation Flying of Small Satellites Using Coulomb Forces," n/d.

[24] Parker, G., et al., "Coulomb Formation Flying," *Michigan Tech: Aerospace and Ocean Engineering Department*, 2006.

[25] Schaub, G., et al., "Challenges and Prospects of Coulomb Spacecraft Formation Control," n/d.

[26] Deshmukh, S., "Controlled Spacecraft Charging for Coulomb Force Control of Spacecraft Formations," *Michigan Technological University*, 2002.

[27] Vasavada, H., and Schaub, H., "Analytic Solutions for Equal Mass Four-Craft Static Coulomb Formation," *Journal of the Astronautical Sciences*, Vol. 56, No. 1, 2008, pp. 17–40.

[28] Joe, H., et al., "Formation Dynamics and Coulomb Satellites," *Michigan Technological University*, n/d.

[29] Seubert, C., and Schaub, H., "Effective Coulomb Force Modeling for Spacecraft in Earth Orbit Plasmas," *Advances in Space Research*, Vol. 54, No. 2, 2014.

[30] Liberzon, D., "Calculus of Variations and Optimal Control Theory," *Princeton University Press*, 2011.